Iterative methods for solving nonlinear ill-posed problem in parameter estimation for electrical impedance tomography

Zhang, Q.

Award date:
2011

Iterative methods for solving nonlinear ill-posed problem in parameter estimation for electrical impedance tomography

Qi Zhang

Eindhoven University of Technology
Department of Mathematics and Computer Science
Centre for Analysis, Scientific Computing and Applications

Iterative Methods for Solving Nonlinear Ill-Posed Problem in Parameter Estimation for Electrical Impedance Tomography

Author:

Qi Zhang

Adviser:

Dr. Michiel Hochstenbach

Committee members: **Dr. Michiel Hochstenbach**

Dr. Jos Maubach

Dr. ir. Remco Duits

Dr.ir. Arris Tijsseling

Eindhoven, July 2011

Acknowledgement

Firstly, it is my distinct pleasure to express my deep sense of gratitude and indebtedness to my supervisor Dr. Hochstenbach, who was indispensable for the completion of this thesis. He is also a good friend who gives me lots of suggestions not only in my project but also in the further study and work.

Secondly, I would like to thank the European School for Industrial Mathematics (ESIM) for offering me a good chance to study the joint master's program in Industrial Mathematics. Going abroad to see the world and study more advanced technology is my dream since I was high school boy. Because of ESIM, I got the opportunity to make my dream true. My great thanks go to the Department of Mathematics and Computer Science, Eindhoven University of Technology, for their outstanding master courses that open the door of industrial mathematics to me. I would like to thank the professors and the staff members of CASA for the great social and academic atmosphere and for the great learning opportunities offered in the past year.

Last but not least, I would like to give my special thanks to my loving parents, who support me whenever I meet any difficulties and my fiancée Xin Zheng, who encourages me all the time. Additionally, I would like to thank my best friend Ruoheng Huang, who has given me much help since I prepared to go abroad three years ago. I also want to thank all my friends who have offered so much support and help during my study and work on the thesis. Special thanks go to Qixiao Yu, Zhengjie Lu, Yabin Fan, Chhitiz Buchasia, Juan Pablo Maldonado and Haik Sedrakian for their constant support during my study in Europe. I want to thank whom has brought all of you into my life, and it makes my life here unforgettable to have friends as you all.

Abstract

Electrical impedance tomography (EIT) is a medical imaging technique in which an image of the conductivity or permittivity of part of the body is inferred from surface electrical measurements. The reconstruction of conductivity distribution from the boundary measurements is the inverse problem which is nonlinear and ill-posed. This thesis firstly studies the mathematical model of EIT and analyzes the nonlinear and ill-posedness of its inverse problem. Then, for solving the problem, it discretizes the forward problem by finite element method. After that, it applies iterative methods to image reconstruction of conductivity. Finally, in simulations and numerical experiments, it discusses efficiency and reconstruction results of methods, and gives some conclusions.

Contents

Chapter 1

Introduction

1.1 Aims and objectives

Electrical impedance tomography (EIT) is a medical imaging technique in which an image of the conductivity or permittivity of part of the body is inferred from surface electrical measurements. However, based on fast development in imaging technology, there are so many ways for us to apply EIT in various areas, especially for medical purpose. Here, one may ask "why we need electrical impedance model since we've already had many advanced technologies in such areas?" There are two main reasons. Firstly, it is a very good technique for the nondestructive testing of materials. Secondly, it is a cheap technique compared with others. Electrical impedance tomography has these advantages because it utilizes simple metal electrodes and other light and cheap instruments.

The most important part of EIT is to reconstruct the distribution of conductivity from the physical measurements i.e., the current and the voltage on the boundary. This is a typical inverse problem. Unfortunately, most of the inverse problems are ill-posed. This means that the solution does not depend continuously on the data. If one wants to apply the numerical methods which are used in solving some well-posed problems to approximate an ill-posed problem, whose solution does not depend continuously on the data, then one will see the results of expectation are not stable, i.e., with oscillations in the solution. Unfortunately, the problem of the reconstructions for EIT is nonlinear and ill-posed, while it is challenging to find the appropriate stable method.

Fortunately, there are some regularized iterative methods providing possibilities for solving our problem. But depending on the different reconstruction problem, i.e., in 2D or 3D, to choose the suitable methods and to find more efficient methods to reconstruct the distribution of conductivity are necessary to study.

This thesis presents a research work on modeling the EIT problem and applying iterative methods for reconstructing conductivity distributions. And this thesis is structured as follows:

•**Chapter 1** briefly introduces the inverse problem and ill-posed problem (linear and nonlinear). It simply presents the methods for solving the ill-posed problem.

•**Chapter 2** firstly introduces the motivation and the work principle of EIT. Then it constructs

the mathematical model for EIT and studies the nonlinear ill-posedness of its inverse problem.

•**Chapter 3** defines the forward problem and the inverse problem of EIT at the beginning, and gives the basic idea of reconstruction of conductivity for EIT. Then it discretize the forward model which is achieved in Chapter 2. Finally, it summarizes the discrete forward model and gives the clue to solve reconstruction in the real simulation.

•**Chapter 4** introduces the basic principles of iterative methods, and then gives the derivations of Newton type methods for the inverse problem of EIT. Additionally, it studies the CG type methods for the problem.

•**Chapter 5** tries to make simulations in two dimensional and three dimensional cases, and then discusses and compares the results based on applying different iterative methods.

•**Chapter 6** is the conclusion of the whole thesis which states the significance of the thesis work and the possible improvements.

1.2 Short introduction of inverse problem

In recent years, the applications of inverse problems in industry have been developed very fast, since the powerful technology of computer is growing rapidly and demands for solving problems from various engineering fields, such as geophysics [1, 2, 3], materials science [4, 5], remote sensing technique [6], pattern recognition [7], imaging processing [8, 9, 10, 11, 12], hydromechanics [13, 14], even the economy fields [15, 16, 17, 18, 19], are increasing quickly.

It is naturally to ask “inverse to what?” when using the term inverse problem. J.B. Keller [20] gave an answer that two problems inverse to each other if the formulation of one problem involves the other one. However, there are, from the applications point of view, two different motivations for studying such inverse problem: first, one wants to know the past states or parameters of a physical system. Second, one wants to find out how to influence a system via its present state or via parameters in order to steer it to a desired state in the future. Thus, one might say the inverse problems are concerned with determining causes for a desired or an observed effect [21].

As we know, most of the inverse problems are not well-posed (ill-posed), which are more complicated in computation and theory compared with well-posed ones. We will see the definition of ill-posed problem in the next part.

1.2.1 Ill-posed problem

In 1923, Hadamard gave the definition for well-posed problem as the below [22]:

Definition 1.1 The problem is well-posed if the following properties hold:
1. For all admissible data, a solution exists.
2. For all admissible data, the solution is unique.
3. The solution depends continuously on the data.

Ill-posed problems which come from inverse problems do not fulfill Hadamard's definition of well-posedness as one above properties.

If a problem is ill-posed, one is usually not too much concerned with the violation of the first property, because we can usually be enforced by relaxing the notion of a solution at least for exact data. Violation of the second property is considered to be much more serious, since one has to decide which solution is interested and has to "invent" additional measurements to solve this problem. Violation of the third one creates serious numerical problem: if one wants to apply the numerical methods which are used in solving some well-posed problems to approximate an ill-posed problem whose solution does not depend continuously on the data, then one will see the results of expectation are not stable, i.e., it is with oscillations.

In fact, the third violation we see above could not be solved completely, however, we can find a (partial) remedy for this, called "regularization methods", which will always be found the right compromise between accuracy and stability.

1.2.2 Nonlinear ill-posed problem and parameter estimation

In fact, ill-posed problems can be classified by two categories. One is linear and the other is nonlinear. For the linear case, we consider a linear operator equitation of the form

$$Tx = y,$$

where T is a linear operator between spaces (i.e., Hilbert space) X and Y. Then, the linear ill-posed problem above does not satisfy Hadamard's definition. Mostly, it violates the third property of Hadamard's definition, although there are also some violations happened to the first and the second ones, which we can solve by generalizing the notion of solution.

Now, we want to deal with the fully nonlinear case, i.e., we want to solve

$$F(x) = y, \tag{1.2.1}$$

where $F : D(F) \subset X \to Y$ is a nonlinear operator between spaces (i.e., Hilbert spaces) X and Y. Under ill-posedness of the nonlinear problem, we mean that the solutions do not depend continuously on the data.

In physical or technical applications, one often has the situation that the physical laws governing the process are known, but quantitative information about physical parameters is not available. The parameter estimation, in general, is a nonlinear inverse problem even if the underlying equation is (for a known parameter) a linear equation (we will see this in the next chapter). So, in our problem, we generally assume

$$F(x^\delta) = y^\delta, \tag{1.2.2}$$

where $y^\delta = y + \delta$ is a collection of discrete observations which contain some amount of noise that may arise from unmodeled influences off instrument readings or numerical round-off. x^δ is the corresponding solution. In our case, it means the approximated parameter. F is a nonlinear operator.

The forward problem is to find the solution of our partial differential equation (PDE) which parameters are known. The inverse problem is to find the parameter by giving the solution of PDE. Because of the violation of third property in Hadamard's definition, the small perturbations or errors from observation data would make our solution very unstable. We need to find the right compromise between accuracy and stability.

1.3 Methods for solving nonlinear ill-posed problems

So far, there are three main directions of research for solving ill-posed problems:

1) Variational methods, including Tikhonov's approach with various means for choosing the regularization parameter (see more [23]);
2) Iterative methods;
3) Methods of statistical regularization (see more [24]).

In this thesis, we concentrate on the second direction for solving our problem, because the efficiency of the methods is illustrated by the solution of numerous applied problems. Among such problems are the most interesting: the problem of image processing, the inverse problem of geophysics, and the problems of computerized tomography within linear and nonlinear models. The problem of tomography can be formulated as the inverse coefficient problem for second-order partial differential equations as we have in our thesis. For variational methods and methods of statistical regularization, we will not consider here, but they are also good directions for future study in parameter estimation of electrical impedance tomography (EIT).

Chapter 2

Electrical impedance tomography model

2.1 Background

2.1.1 Motivation of EIT

In recent years, based on fast development in imaging technology, there are so many ways for us to apply EIT in various areas, especially the medical direction. Here, one may ask “why we need electrical impedance model since we’ve already had many advance technologies in such area?” There are two main reasons.

Firstly, it is a very good technique in nondestructive testing of materials. The most common medical imaging technique uses X rays, called X-ray imaging, where X rays travel in straight lines through the body and cause darkening of photographic film behind the body. Its films have excellent spatial resolution. However, X rays are damaging to tissue and may cause cancer [11].

Secondly, it is a cheap technique compared with others. For example, a very famous instrument is the computerized tomography (CT). Although, it has excellent spatial resolution, it is large and expensive. Another example, magnetic resonance imaging (MRI), images the distribution of certain chemicals, such as the hydrogen in water. The patient is placed in a strong magnetic field. The processing of the hydrogen atoms is scanned with an oscillating electric field to yield the distribution with excellent spatial resolution. The instrument is very large and expensive, although there is no damage to the patient.

Therefore, we need a reasonably cheap and relatively simple instrument for our medical imaging as well as nondestructive testing. Electrical impedance tomography could do this because it utilizes simple metal electrodes and other light and cheap instruments.

2.1.2 Principles of EIT

From biology point of view, we know that in biological tissue the electrical conductivity and permittivity vary between tissue types likewise depending on temperature and physiological factors. So this means there are some possibilities to achieve the distribution of impedance in space by testing current and voltage. Electrical impedance tomography (EIT) is a medical

imaging technique in which an image of the conductivity or permittivity of part of the body is inferred from surface electrical measurements. Typically, conducting electrodes are attached to the skin of the subject and small alternating currents are applied to some or all of the electrodes. The resulting electrical potentials are measured, and the process may be repeated for numerous different configurations of applied current. Finally, we can reconstruct the image of impedance by these data using techniques of reconstruction. In a word, the principles behind EIT is that by applying a constant current across a material, the voltage distribution resulting on the surface will reflect the internal resistivity distribution.

There is a simple example to illustrate working principle of EIT which is called opposite method model (Hua, Webster, and Tompkins, 1987). Figure 2.1.1 [29] shows a simple EIT diagram with 16 electrodes around the perimeter of a circular medium. In this setup the current I is applied across a pair of electrodes on the opposite sides of the core while the voltage distribution V_i is measured between each set of the neighboring electrodes. After the voltage around the entire perimeter has been measured, the current drive electrodes are rotated to the neighboring electrode, such that they remain opposite, and the voltage at all electrodes is measured once again. This process continues until the $12 \times 16=192$ sets of voltage measurements are complete.

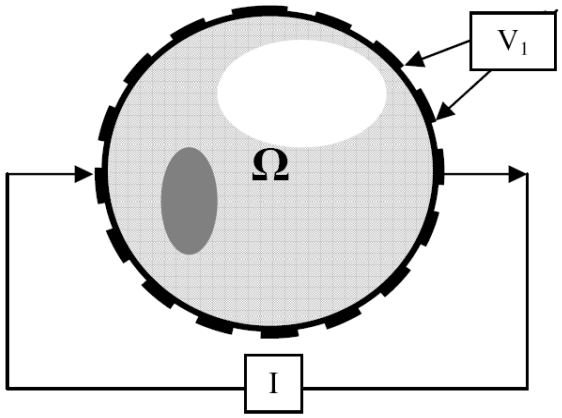

Figure 2.1.1 Model of EIT

Figure 2.1.2 [30] also shows the process of this model. The figure A in Figure 2.1.2 shows the first step, we achieve the data. The figure B in Figure 2.1.2 illustrates the next step we test. The current distribution in this method is more uniform and, therefore, has a good sensitivity.

There is another data collection method which is called neighboring method. The current is applied through the neighboring electrodes and the voltage is measured successively from all other adjacent electrode pairs. Figure 2.1.3[30] illustrates the application of this method for a cylindrical volume conductor with 16 equally spaced electrodes. The figure A in Figure 2.1.3 shows the first step, we achieve the data of voltage. The figure B in Figure 2.1.2 illustrates the next step where we change the electrodes where we inject the current. The whole process continues until the $13 \times 16=208$ sets of voltage measurements are complete.

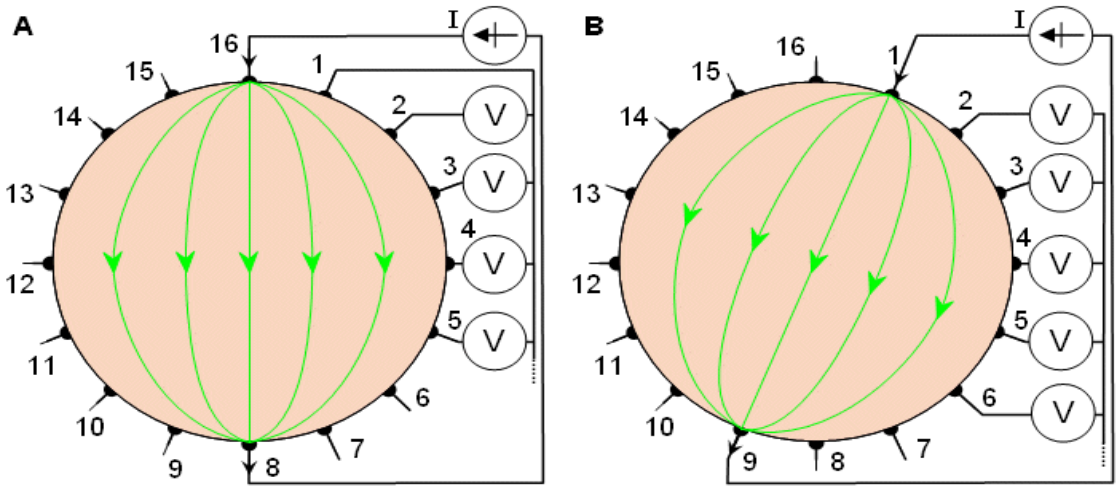

Figure 2.1.2 Opposite method

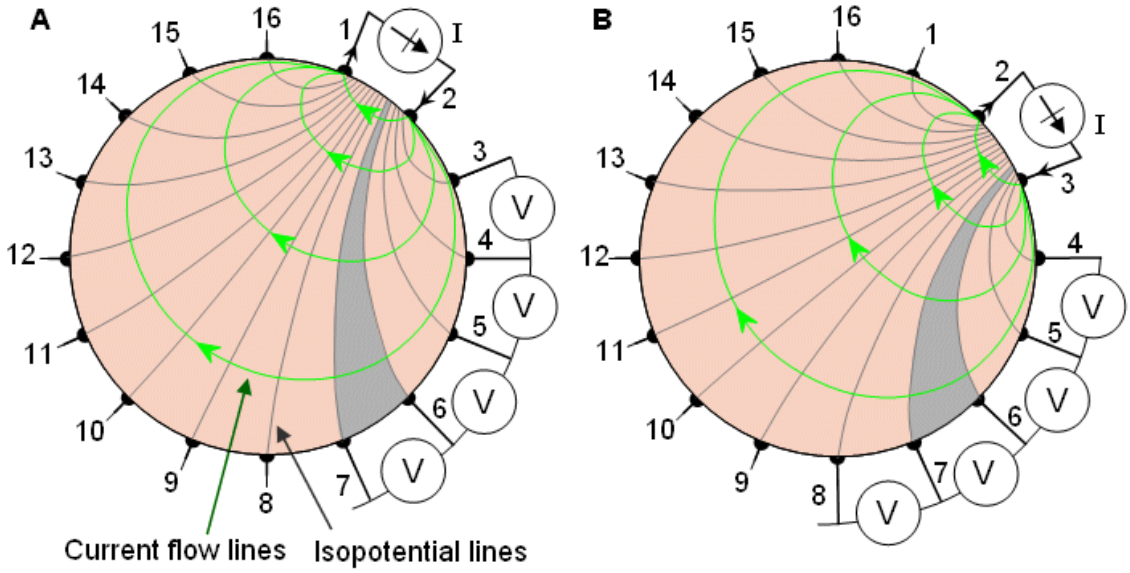

Figure 2.1.3 Neighboring method

EIT is useful for monitoring patient lungs because the air has a large conductivity contrast to the other tissues in the thorax. The most promising clinical application of lung EIT measurements is for monitoring patients being treated with mechanical ventilation. Such ventilation can often result in ventilator-associated lung injury. EIT can resolve the changes in the distribution of lung volumes between the dependent and the non-dependent lung regions as ventilator parameters are changed. Thus, EIT measurements may be used to control the specific ventilator settings to maintain lung protective ventilation for each patient.

The model can be illustrated as in Figure 2.1.4. [31]. Small alternating electrical currents were injected through pairs of adjacent electrodes in a rotating mode. After each current injection, the resulting potential differences were measured between adjacent pairs of remaining

electrodes. By the end of a complete cycle of current injections through all 16 electrode pairs, a set of 208 values of surface potential differences was collected. The data were acquired at a rate of 13 cycles/s. The individual measurements consisted of 1500 measuring cycles and were always initiated 30 s before the pull-up phase.

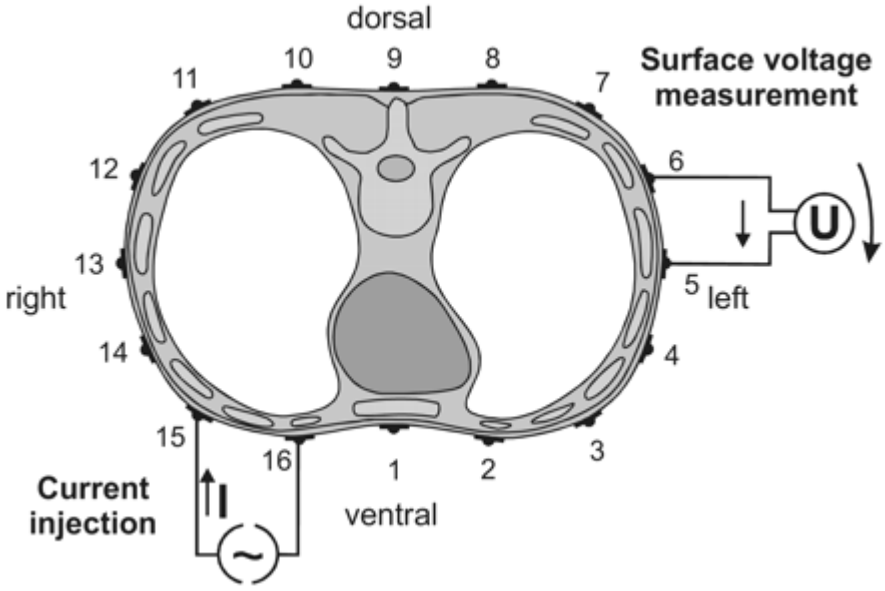

Figure 2.1.4

The above images are from the EIT group at Oxford Brookes University and depict an early attempt at three dimensional EIT imaging of the chest using the OXBACT3 EIT system. The reconstructed image is a time average and shows lungs as low conductivity regions. Figure 2.1.5 shows a work process of EIT.

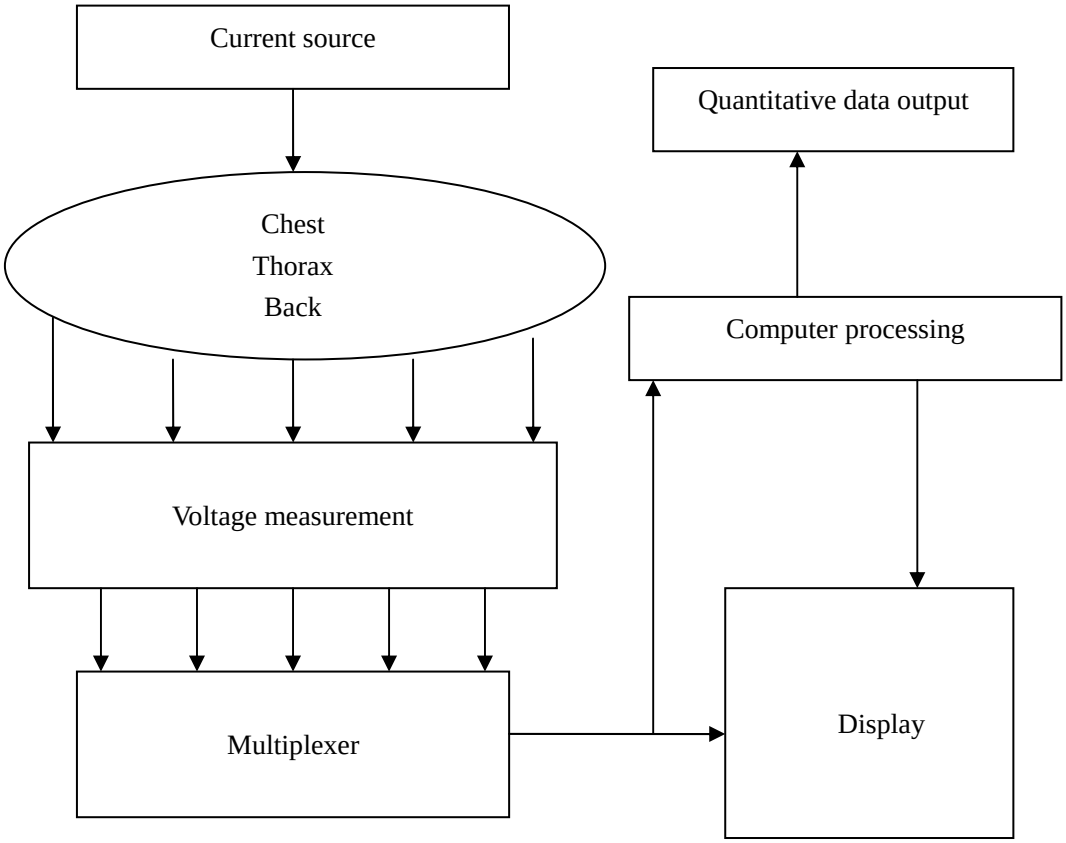

Figure 2.1.5

2.2 Mathematical modeling for EIT

2.2.1 Objective of Modeling

As we introduced, the aim of EIT is to reconstruct the conductivity (or resistivity, admittivity) distribution in the interior of a volume. To achieve this, deriving equations which relate to this parameter is very important. Assuming, if we know the parameter of conductivity in space, by physical laws, we have equations that can calculate the electric field in its interior when known current patterns are driven from its boundaries. In fact, we can calculate the potential distribution in the interior or at the surface of the conductive volume. So, it is natural to consider that we can estimate our unknown parameter of conductivity in space from potential at the surface which could be measured. We know that the former is the forward problem and latter is the inverse problem.

Therefore, the reconstruction of conductivity distribution is the inverse problem. Actually, to

have the model of inverse problem, we need to derive the physical model of the forward problem firstly. This is the main task we will do in the next section.

2.2.2 The physical model of forward problem

To model the physical equations, we need an accurate model of the volume (considering in 3D). For example, we need to know, the boundary geometry, structural characteristics of the physical volume, the boundary electrodes, location, contact impedance and shape. Once a real model is created, we begin to apply mathematical tool to formulate this model. In this section, we assume that the distribution of conductivity γ is known and then formulate the model which reflects the relations between γ and other physical parameters.

The first physical model is a Laplacian equation derived from Maxwell's equations for electro-magnetics [25]. In the following equations, E is the electric field, B the magnetic field, ρ the charge density, J the current density, ν the outward unit normal vector, c the speed of light and ε_0 the constant.

For a conductive isotropic volume $\Omega \in R^3$ enclosed by a fixed C^2 smooth boundary $\partial\Omega$, in microscopic Maxwell's equations, Gauss's law states that the flux of E through a closed surface equals the total charge density inside divided by ε_0.

$$\nabla \cdot E = \frac{\rho}{\varepsilon_0} \tag{2.2.1}$$

In addition, Maxwell–Faraday equation presents that the line integral of E around a loop is equal to the negative rate of change of the flux of B through the loop, yielding

$$\nabla \times E = -\frac{\partial B}{\partial t} \tag{2.2.2}$$

The flux of B through a closed surface is equal to zero by Gauss's law for magnetism,

$$\nabla \cdot B = 0 \tag{2.2.3}$$

and Ampère's circuital law introduces the integral of B around a loop is equal to the current flowing through the loop plus the rate of change of the flux of E through the loop divided by the constant ε_0, yielding

$$\nabla \times B = \frac{J}{\varepsilon_0} + \frac{\partial E}{\partial t} \tag{2.2.4}$$

In EIT, the excitation conditions are quasi-static as the driving patterns are time harmonic AC signals at a low frequency ω. But we can assume they are static if the measurements for each pattern are considered to be collected instantaneously. Therefore,

$$\frac{\partial E}{\partial t} \approx 0, \quad \frac{\partial B}{\partial t} \approx 0 \tag{2.2.5}$$

Using these, equation (2.2.2) becomes

$$\nabla \times E = 0 \tag{2.2.6}$$

This means that there exists a scalar u whose gradient is equal to the vector E when the curl of it is equal to zero, in particular

$$E = -\nabla u \tag{2.2.7}$$

When 'static' current are injected, under the assumptions (2.2.5), equation (2.2.4) becomes

$$\nabla \times B = \frac{J}{\varepsilon_0} \tag{2.2.8}$$

In these conditions, the current density J can be assumed to be time invariant. If I_n is the n'th current pattern driven into the volume, for a boundary electrode surface s, then we have

$$I_n = \int_s J \cdot \nu ds \tag{2.2.9}$$

From the charge conservation law, if S is the surface of $\partial\Omega$,

$$\int_S J \cdot dS = -\frac{d}{dt}(Q_\Omega) \tag{2.2.10}$$

The charge in the interior of the volume Q_Ω can be expressed as a volume integral of the charge density as

$$Q_\Omega = \int_\Omega \rho dV \tag{2.2.11}$$

Combining (2.2.11), (2.2.9) and (2.2.10) yields,

$$\nabla \cdot J = -\frac{\partial \rho}{\partial t} \tag{2.2.12}$$

This is another expression of the charge conservation theorem, according to which the flux of the current flowing through a closed surface is equal to the negative rate of change of charge density in the interior. Because there are no current sources in the interior of the volume and E does not change with time, the right hand side of the equation (2.2.12) can be se to zero

$$\nabla \cdot J = 0 \tag{2.2.13}$$

In a linear isotropic medium the current density and the electric field are related by the approximation

$$J \approx \gamma E \approx (\sigma + i\omega\varepsilon)E \tag{2.2.14}$$

where σ is the electrical conductivity, ε the electrical permittivity and γ the complex conductivity of the medium [25], substituting (2.2.14) into (2.2.13) leads to

$$\nabla \cdot \gamma E = 0 \tag{2.2.15}$$

which combined with (2.2.7) yields the Laplacian elliptic partial differential equation

$$\begin{aligned} \nabla \cdot \gamma(-\nabla u) &= 0 \\ \nabla \cdot (\gamma \nabla u) &= 0 \end{aligned} \tag{2.2.16}$$

The mixed (Dirichlet and Neumann) boundary conditions accompanying the Laplacian equation (2.2.16) are known as the complete electrode model (CEM) [26], [27]. If $\Gamma_1 \subset \partial\Omega$ is the subset of the surface of the volume underneath the electrodes, then the corresponding current density is

$$\gamma \frac{\partial u}{\partial \nu} = J \text{ on } \Gamma_1 \tag{2.2.17}$$

while for the rest of the surface $\Gamma_2 = \partial\Omega \setminus \Gamma_1$,

$$\gamma \frac{\partial u}{\partial \nu} = 0 \text{ on } \Gamma_2 \tag{2.2.18}$$

In addition, for each of the electrodes the integral of the current density over the whole

electrode surface s is equal to the total amount of the current I_l flowing to or from that electrode,

$$\int_{E_l} Jds = \int_{E_l} \gamma \frac{\partial u}{\partial \nu} ds = I_l \qquad l = 1, ..., L. \tag{2.2.19}$$

where L is the number of electrodes in the system and $E_l \subset \partial\Omega$. Finally, the value of potential V_l measured on the l'th electrode is equal to the sum of the potential on the boundary surface underneath that the electrode and the potential drop across the electrode's contact impedance z_l [Ω/m^2],

$$u + z_l \gamma \frac{\partial u}{\partial \nu} = V_l \qquad l = 1, ..., L. \tag{2.2.20}$$

The model has been proved to have a unique solution [28] when the charge conservation theorem

$$\int_{\partial\Omega} J = 0 \Leftrightarrow \sum_{l=1}^{L} I_l = 0 \tag{2.2.21}$$

is considered, and a choice of ground is made, i.e.,

$$\int_{\partial\Omega} u = 0 \Leftrightarrow \sum_{l=1}^{L} V_l = 0 \tag{2.2.22}$$

Finally, we summarize our EIT model, which is also called the complete electrode model (CEM) [32], as

$$\nabla \cdot (\gamma \nabla u) = 0 \text{ in } \Omega$$

with Neumann boundary condition,

$$\gamma \frac{\partial u}{\partial \nu} = J \text{ on } \Gamma_1$$

Here, J is the corresponding current density which is underneath the electrodes, with measure of the total amount of current I_l on the l'th electrode,

$$\int_{E_l} \gamma \frac{\partial u}{\partial \nu} ds = I_l \qquad l = 1, ..., L.$$

The value of the potential V_l measured on the l'th electrode is

$$u + z_l \gamma \frac{\partial u}{\partial \nu} = V_l \qquad l = 1, ..., L.$$

Additionally, uniqueness conditions reads

$$\int_{\partial\Omega} J = 0 \Leftrightarrow \sum_{l=1}^{L} I_l = 0$$

$$\int_{\partial\Omega} u = 0 \Leftrightarrow \sum_{l=1}^{L} V_l = 0$$

2.3 Nonlinear ill-posedness of parameter estimation

As we discussed in the last chapter, in general, parameter identification is a nonlinear inverse problem. For simplicity, let Ω = [0 1], Γ_1 = {0}. Consider the following one-dimensional boundary value problem of EIT model we have in the last section. We want to find $u(x)$ such that

$$(\gamma(x)u_x)_x = 0 \text{ in } \Omega \tag{2.3.1}$$

with Neumann boundary condition,

$$\gamma(x)u_x(x) = J_0 \text{ on } \Gamma_1 \tag{2.3.2}$$

The problem above is a norm boundary value problem. The question is how to determine $\gamma(x)$ from internal measurements of the voltage $u(x)$ and boundary measurements of the current density J_0.

Then applying integral to two sides of equation (2.3.1), we have

$$\int_0^x (\gamma(s)u_s)_s ds = 0 \tag{2.3.3}$$

and applying boundary conditions (2.3.2) into (2.3.3) yields

$$\gamma(x) = \frac{\gamma(0)u_x(0)}{u_x(x)} = \frac{J_0}{u_x(x)} \tag{2.3.4}$$

Thus, in order to compute γ, we have to differentiate the data u, which is an ill-posed problem as the following explanation.

Considering $u \in C^1[0,1]$ be any function, $\delta \in (0,1)$, $n \in N$ $(n \geq 2)$ be arbitrary, and defining

$$u_n^\delta(x) := u(x) + \delta \sin(\frac{nx}{\delta}), \qquad x \in [0,1] \tag{2.3.5}$$

Then, we obtain

$$(u_n^\delta)'(x) = u'(x) + n\cos(\frac{nx}{\delta}), \qquad x \in [0,1] \tag{2.3.6}$$

So, in the uniform norm,

$$\left\|u - u_n^\delta\right\|_\infty = \delta \tag{2.3.7}$$

however,

$$\left\|u' - (u_n^\delta)'\right\|_\infty = n \tag{2.3.8}$$

Hence, if we consider u the exact data, u_n^δ is the data with error δ. Then for an arbitrary small data error δ, the error in the result of derivative can be arbitrarily large. Therefore, the derivative does not depend continuously on the data with respect to the uniform norm.

Return to our inverse problem which determines the parameter γ in (2.3.4). Firstly, differentiating the data u is an ill-posed problem as explained above. Additionally, another effect of instability comes from the division by u_x. For example, errors in J_0 (It will have

errors because we achieved the data by instruments) are amplified when u_x is smaller than 1 in some regions. Therefore, some instability has to be expected where u_x is small. This is a nonlinear effect.

After all discussions in this chapter, we could see that parameter estimation for EIT is a nonlinear ill posed problem. We need tools to solve the nonlinear ill-posed problem.

Chapter 3

The Forward Problem

3.1 Definition of the forward problem

After we construct the model of EIT in the last chapter, for reconstructing our parameter distribution, we need to define our forward problem (or forward non-linear mapping) mathematically.

3.1.1 Dirichlet-to-Neumann map and Neumann-to-Dirichlet map

Before giving definition of the forward problem, we need to simply introduce the definitions of Dirichlet-to-Neumann map (D-N map) and Neumann-to-Dirichlet map (N-D map) for our EIT model. For more details, see references [33, 34, 35, 36, 37, 38, 39, 40, 41, 42].

Definition 3.1 The Dirichlet-to-Neumann map associated to γ or voltage-to-current map is

$$\Lambda_\gamma : u\,|_{\partial\Omega} \in H^{1/2}(\partial\Omega) \mapsto \gamma\frac{\partial u}{\partial \nu}\,|_{\partial\Omega} \in H^{-1/2}(\partial\Omega)$$

where $u \in H^1(\Omega)$ solves the Dirichlet problem,

$$\begin{cases} L_\gamma u = 0 & in \quad \Omega \\ u = V & on \quad \partial\Omega \end{cases} \tag{3.1.1}$$

where, $L_\gamma u := \nabla \cdot \gamma \nabla u$, V is the voltage on the boundary.

Definition 3.2 The Neumann-to- Dirichlet map associated to γ or current-to-voltage map is

$$N_\gamma : \gamma\frac{\partial u}{\partial \nu}\,|_{\partial\Omega} \in H^{-1/2}(\partial\Omega) \mapsto u\,|_{\partial\Omega} \in H^{1/2}(\partial\Omega)$$

where $u \in H^1(\Omega)$ solves the Neumann problem,

$$\begin{cases} L_\gamma u = 0 & in \quad \Omega \\ \gamma\frac{\partial u}{\partial \nu} = J & on \quad \partial\Omega \\ \int_{\partial\Omega} u = 0 \end{cases} \tag{3.1.2}$$

where J is the current density on the boundary.

3.1.2 The forward nonlinear mapping

In many books, it is general to determine conductivity γ from boundary measurements by considering the Dirichlet-to-Neumann map. However, in many applications of EIT especially

in medical imaging, rather than the Dirichlet-to-Neumann map (D-N map), one should consider the Neumann-to-Dirichlet map (N-D map). That is, the map associating to specified current densities supported on a portion $\Gamma_1 \subset \partial\Omega$ the corresponding boundary voltages, also measured on the same portion Γ_1 of $\partial\Omega$. In fact, we mean this Γ_1 is referred as in the last chapter (2.2.17). And the rest of the portion is $\Gamma_2 = \partial\Omega \setminus \Gamma_1$, where there is no electrode.

In this thesis, for the finite approximation of the forward problem the Galerkin formulation is used. In this, the admissible measurements and solutions are considered to belong to the Hilbert spaces, and the forward nonlinear mapping is formalized as,

$$F : \gamma\,|_{\Omega} \mapsto V\,|_{\partial\Omega} \tag{3.1.3}$$

hence given a model, the forward operator F can also be thought of as a Neumann-to-Dirichlet operator associated with γ,

$$F(\gamma) = V \tag{3.1.4}$$

3.2 The inverse problem

As we discussed in the last section, we have the definition for the forward problem whose parameter is known. Figure 3.2.1 shows the definition of the forward problem. Given the conductivity distribution with boundary current density, we need to solve for the voltage on the boundary.

Figure 3.2.1 The forward problem

So far, we understand the forward problem clearly. The inverse problem for complete data (given measured voltage on the boundary with noise data, i.e., $V^{\delta}_{measure}$) is then the recovery of γ^{δ} from F (also we can say from N-D map). Here, γ^{δ} is the corresponding conductivity related measured voltage on the boundary with noise level δ. Figure 3.2.2 shows the definition of the inverse problem.

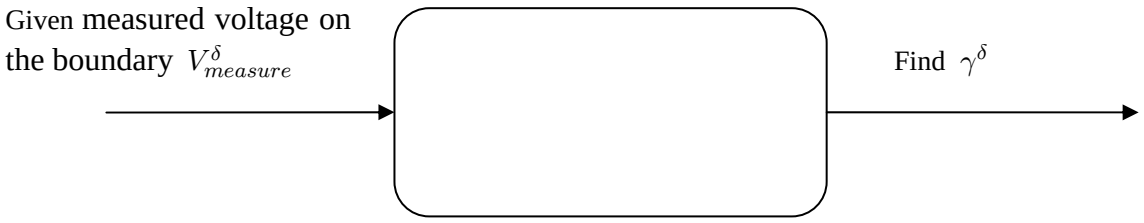

Figure 3.3.2 The inverse problem

3.3 The idea of reconstruction of conductivity for EIT

In our real experiments, we could actually achieve the data of voltage and current on the boundary. The problem is how to recover our conductivity γ in Ω from these known physical measurements.

The basic idea of reconstruction is to repeatedly solve the forward problem while updating γ according to some criteria. For example, it is natured to consider the criterion is based on minimizing the norm of the difference between calculated voltage on the boundary V and the measured voltage $V^{\delta}_{measure}$ on the boundary which includes the noise data δ, as the below,

$$f(\gamma) = \frac{1}{2}(F(\gamma) - V^{\delta}_{measure})^{*}(F(\gamma) - V^{\delta}_{measure}) = \frac{1}{2}\left\|F(\gamma) - V^{\delta}_{measure}\right\|_2^2 \qquad (3.3.1)$$

There are two reasons for considering this criterion. Firstly, F is N-D mapping associated with γ. It reflects the relation between our conductivity in the domain and voltage on the boundary. Secondly, we normally hope that the corresponding calculated γ^{δ} makes the result of forward problem, i.e., $F(\gamma^{\delta}) = V^{\delta}$, close to the real measured voltage data $V^{\delta}_{measure}$ on the boundary as much as possible. And we may say this γ^{δ} is close to our real one $\gamma^{\dagger}$ while the noise data δ is decreasing to zero. Here, we do not say 'definitely' because it is non-linear mapping which needs more a-priori information to constraint our calculated solution to real solution. See more details in [21]. However, the main principle is to find the γ which lets our calculated voltage approximate to the real one.

The summary of our idea of the algorithm is,

1. Given initial guess of γ^{δ}_0.
2. For k=0, 1, 2…,
3. Calculate $F(\gamma^{\delta}_k) = V_k$
4. If $\left\|F(\gamma^{\delta}_0) - V^{\delta}_{measure}\right\| < \varepsilon$, stop
5. else, update γ^{δ}_k, i.e., $\gamma^{\delta}_{k+1} = \gamma^{\delta}_k + \Delta\gamma^{\delta}_k$
6. Go to step 3

In step 5, the method of updating is corresponding with our criteria or minimizing objective functional. And in this thesis, we consider iterative methods to minimizing our objective functional which will be introduced in the next chapter. Figure 3.3.1 shows the idea of reconstruction.

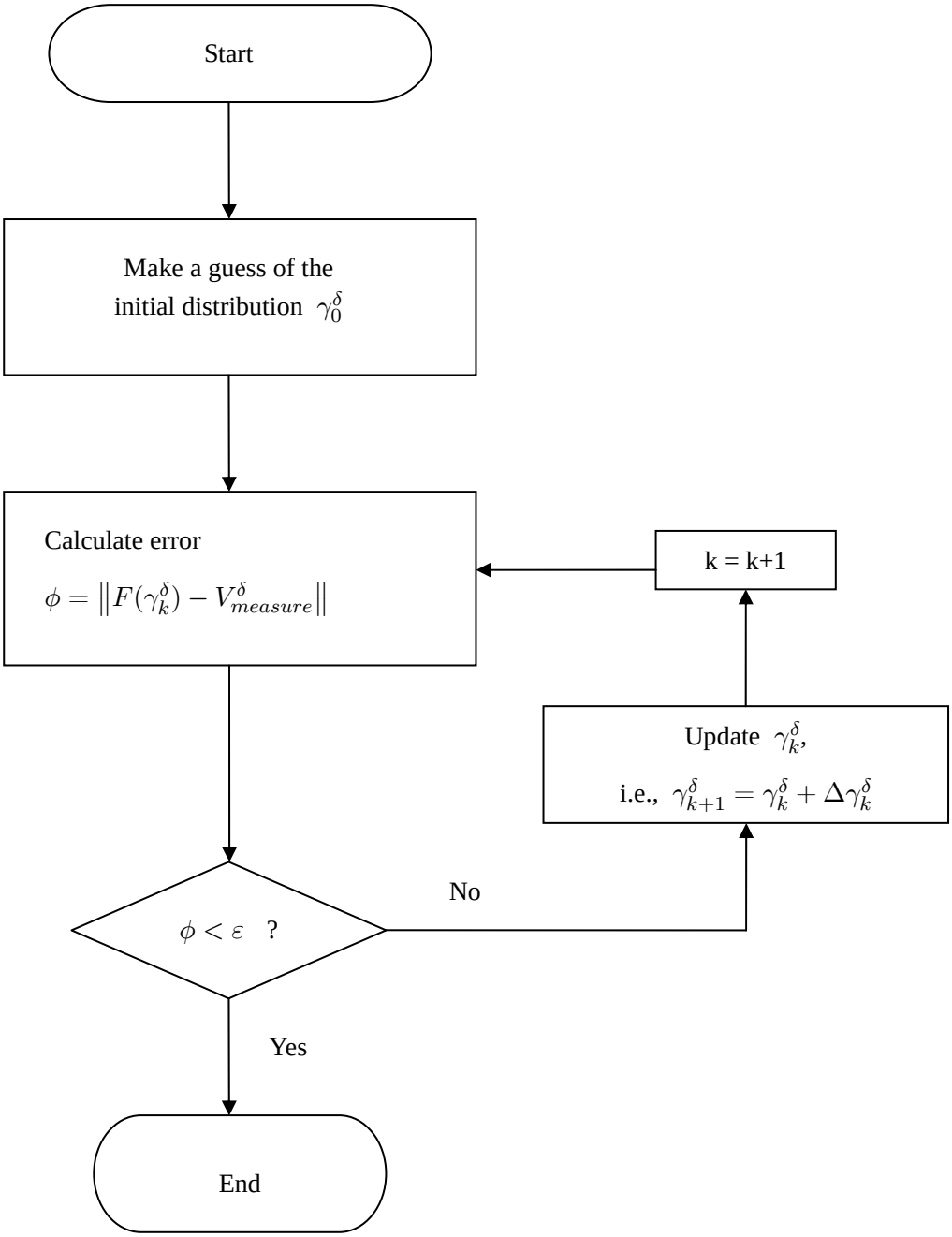

Figure 3.3.1 The flow of reconstruction algorithm

3.4 Discrete approximation for the forward problem

3.4.1 Choice of approximation methods

For the reconstruction of conductivity distribution, we need to solve the forward problem during the calculations. Since we cannot analytically solve the forward problem for an arbitrary distribution, we should use a numerical technique such as the Finite Difference Method (FDM), Finite Element Method (FEM), or Finite Volume Method (FVM). All have been used in EIT problems. However, we choose FEM since there are several advantages as below [44],

1) The mesh can be adapted to a general boundary surface and to the shape and location of electrodes, whereas regular girds in FDM or FVM can result in more efficient computation, traded off against the fine discretization needed to represent irregular boundaries.
2) The FEM gives a piecewise approximation to the governing equations whereas the FDM gives a pointwise approximation.

Therefore, most reconstruction algorithms in EIT use the FEM in solving the forward problem.

In the FEM, the transformation from the continuous domain and integral operator functions to the discrete domains and matrix operators is achieved by some numerical integral approximation methods such as the Quadrature and Galerkin methods [44]. In the next sections, we will derive our forward problem into discrete formulation.

3.4.2 Variational formulation of the forward problem

Before applying the Galerkin method, the weak variational formulation of the forward problem must be derived. In this section, we will use the set of equations (2.2.16) to (2.2.22) and consider our problem in 3D case (real model).

Variational formulation:

Let our test function $v \in V = H^1(\Omega)$, then the following steps can be performed:

- Multiplication with a test function v and integration over the domain Ω for equation (2.2.16):

$$\int_{\Omega} \nabla \cdot (\gamma \nabla u) v dx = 0 \tag{3.4.1}$$

- Integration by parts (i.e., using Green's formula):

$$\int_{\partial\Omega} v(\gamma \nabla u) \cdot \vec{n} ds - \int_{\Omega} (\gamma \nabla u) \cdot \nabla v dx = 0 \tag{3.4.2}$$

where $\vec{n}$ is the outer norm of the surface $\partial\Omega$.

- Incorporating the boundary condition.

This part we need to discuss the two cases. One is the case for the part which does not have contact with electrode. Another one is the case for the rest part which has elements underneath

the electrode. In 3D case, we assume our finite element model with k first-order tetrahedral elements, n vertices and L boundary electrodes. And for an element underneath the electrode l, let Ω_{E_l} be the volume of the element and $\partial\Omega_{E_l}$ is the triangular face shared with the electrode.

For the first case by incorporating the boundary condition (2.2.18) into (3.4.2):

$$\int_{\Omega\setminus\Omega_E} (\gamma\nabla u)\cdot\nabla v dx = 0 \tag{3.4.3}$$

where $\Omega_E = \bigcup_{l=1}^{L} \Omega_{E_l}$.

For the second case by incorporating the boundary condition (2.2.20) into (3.4.2):

$$\sum_{l=1}^{L}\int_{\Omega_{E_l}} (\gamma\nabla u)\cdot\nabla v dx = \sum_{l=1}^{L}\int_{\partial\Omega_{E_l}} v\frac{1}{z_l}(V_l - u)ds \tag{3.4.4}$$

where z_l is the contact impedance of the electrode l and V_l the potential measured on it.

After we incorporate the boundary conditions of (2.2.18) and (2.2.20), additionally, to set the boundary condition (2.2.19), we should consider that in general more than one element will share with a face with an electrode. Assuming that m elements are located underneath the l'th electrode as

$$\partial\Omega_{E_l} = \bigcup_{i=1}^{m} \partial\Omega_{E_l^i} \tag{3.4.5}$$

then

$$\begin{aligned} I_l &= \int_{\Omega_{E_i}} \frac{1}{z_l}(V_l - u)ds = \sum_{i=1}^{m}\int_{\partial\Omega_{E_l^i}} \frac{1}{z_l}(V_l - u)ds \\ &= \frac{1}{z_l}\left|E_l\right| V_l - \sum_{i=1}^{m}\int_{\partial\Omega_{E_l^i}} \frac{1}{z_l} u ds \end{aligned} \tag{3.4.6}$$

where $|E_l|$ is the area of the face of the electrode. Equation (3.4.6) illustrates that the current I_l injected by the l'th electrode, is partly dissipated as power loss across the electrode's contact impedance, and the rest of it is used to generate the potential in the interior of the volume.

So far, gathering all equations (3.4.3), (3.4.4) and (3.4.6), we have the complete variational formulation which is incorporating with all boundary conditions. Then the next step is to apply Galerkin methods.

3.4.3 Galerkin method for discretizing the forward problem

Upon what we got, we assume that u_h is the weak solution to the problem and $\phi_i(x)$ are some piecewise linear basis functions with local support such that

$$\phi_i(x) = \begin{cases} 1 & \text{on vertex i,} \\ 0 & \text{otherwise.} \end{cases} \tag{3.4.7}$$

Then u_h can be expressed as

$$u_h = \sum_{j=1}^{n} u_j \phi_j \tag{3.4.8}$$

And the test function can be expressed as

$$v_h = \sum_{i=1}^{n} v_i \phi_i \tag{3.4.9}$$

For the FEM derivations, the discrete conductivity distribution vector $\gamma \in C^k$ is taken as

$$\gamma = \sum_{i=1}^{k} \gamma_i \psi_i \tag{3.4.10}$$

where

$$\psi_i(x) = \begin{cases} 1 & \text{on element i,} \\ 0 & \text{otherwise.} \end{cases} \tag{3.4.11}$$

are some piecewise constant basis functions. Substituting (3.4.9) into (3.4.3) yields

$$\int_{\Omega \setminus \Omega_E} (\gamma \nabla u_h) \cdot \nabla \phi_i dx = 0, \ i = 1, \ldots, n \tag{3.4.12}$$

Then, substituting u_h from (3.4.8) leads to

$$\int_{\Omega \setminus \Omega_E} \gamma (u_j \nabla \phi_j \cdot \nabla \phi_i) dx = 0 \tag{3.4.13}$$

with $i, \ j = 1, \ldots, n$.
Substituting (3.4.9) into (3.4.4) yields

$$\sum_{l=1}^{L} \int_{\Omega_{E_l}} (\gamma \nabla u_h) \cdot \nabla \phi_i dx = \sum_{l=1}^{L} \int_{\partial \Omega_{E_l}} \phi_i \frac{1}{z_l} (V_l - u_h) ds \ \ i = 1, \ldots, \ n \tag{3.4.14}$$

then, substituting u_h from (3.4.8) leads to

$$\sum_{l=1}^{L} \int_{\Omega_{E_l}} \gamma (u_j \nabla \phi_j \cdot \nabla \phi_i) dx = \sum_{l=1}^{L} \int_{\partial \Omega_{E_l}} \phi_i \frac{1}{z_l} (V_l - u_j \phi_j) ds \tag{3.4.15}$$

with $i, \ j = 1, \ldots, \ n$.
Or,

$$\int_{\Omega_{E_l}} \gamma(u_j \nabla\phi_j \cdot \nabla\phi_i)dx = \int_{\partial\Omega_{E_l}} \phi_i \frac{1}{z_l}(V_l - u_j\phi_j)ds \tag{3.4.16}$$

with l = 1,…, L.

Substituting (3.4.8) into the boundary condition (3.4.6) yields

$$I_l = \frac{1}{z_l}|E_l|\,V_l - \sum_{i=1}^{m} \frac{1}{z_l} u_j \int_{\partial\Omega_{E_l^i}} \phi_j ds \quad j = 1, \ldots, n \tag{3.4.17}$$

Assembling equations (3.4.13), (3.4.16) and (3.4.17), we have the complete Galerkin discretization formulation for our forward problem.

3.4.4 Matrix formulation for the forward problem

Upon all we achieved from last section, in real simulation, we need to transform our problem into matrix form in order to calculate in computer. Generalizing equation (3.4.13) and (3.4.16) for the n'th element, the global conductance matrix is assembled by the following entries for each of the elements.

Assume, local matrices are $A_m \in R^{4\times4}$, $A_z \in R^{4\times4}$ and $A_v \in R^{4\times4}$, which arise from the various factors of (3.4.13) and (3.4.16). The local matrices are

$$A_m(i,j) = \int_{\Omega_E} \gamma(u_j \nabla\phi_j \cdot \nabla\phi_i)dx = \int_{\Omega\setminus\Omega_E} \gamma(u_j \nabla\phi_j \cdot \nabla\phi_i)dx \tag{3.4.18}$$

$$i,\ j = n_1,\ldots,n_4$$

$$A_z(i,j) = \int_{\partial\Omega_{E_l}} \frac{1}{z_l}\phi_i\phi_j ds \quad i,\ j = n_1,\ldots,n_4 \tag{3.4.19}$$

$$A_v(i,j) = \int_{\partial\Omega_{E_l}} -\frac{1}{z_l}\phi_i ds \quad i,\ j = n_1,\ldots,n_4 \tag{3.4.20}$$

where, $n_1,\ldots,n_4$ are the four vertices in each element. If $\overline{u} \in R^4$ is the vector of the potential values at $n_1,\ldots,n_4$, then in each element, the following relation holds by equations (3.4.18) to (3.4.20),

$$(A_m + A_z)\overline{u} + A_v V_l = 0 \tag{3.4.21}$$

The local matrix form of (3.4.17) is illustrated as the below:
Firstly, we have

$$I_l = \frac{1}{z_l}|E_l|\,V_l - \sum_{i=1}^{m} \frac{1}{z_l} u_j \int_{\partial\Omega_{E_l^i}} \phi_j ds \quad j = n_1,\ldots,n_4 \tag{3.4.22}$$

Then, for the last term of (3.4.22) we've already had the local matrix form as (3.4.20). For the

part of $\frac{1}{z_l}|E_l|V_l$, the functional $\frac{1}{z_l}|E_l|$ multiplying V_l in (3.4.22) forms the diagonal compartment $A_D \in R^{L\times L}$, which is the global conductance matrix in (3.4.25). Define estimates of the contact impedance for each electrode,

$$A_D(i,j) = \begin{cases} \left(\frac{1}{z_l}\right)_j |E_l| & \text{for i=j} \\ 0 & \text{otherwise} \end{cases} \quad i,j = 1,\ldots,L \tag{3.4.23}$$

Therefore, the local matrices of (3.4.22) yields

$$A_v\overline{u} + A_D V_l = I_l \tag{3.4.24}$$

Finally, we assemble the local relations of matrices (3.4.21) and (3.4.24), and have the global matrix A and its system of linear equations as

$$\begin{bmatrix} A_M + A_Z & A_V \\ A_V^T & A_D \end{bmatrix} \begin{bmatrix} U \\ V_L \end{bmatrix} = \begin{bmatrix} 0 \\ I^d \end{bmatrix} \tag{3.4.25}$$

where,

$$A = \begin{bmatrix} A_M + A_Z & A_V \\ A_V^T & A_D \end{bmatrix} \tag{3.4.26}$$

$A_M \in R^{n\times n}$ is assembled from the local A_m matrices; $A_Z \in R^{n\times n}$ is assembled from the local A_z matrices; $A_V \in R^{n\times L}$ is assembled from the local A_v matrices; $A_V^T \in R^{L\times n}$ is the transpose of A_V. $U \in R^n$ is the nodal potential distribution and $V_L \in R^L$ is the potential values on the boundary electrodes. I^d is a finite set of current patterns.

3.5 Summary

In section 3.1.2, we defined the forward operator. After discretizing the forward problem, we could derive the discretized operator for our forward problem in order to simulate in the numerical experiments.

From (3.4.25), it is equivalent to the following,

$$\begin{bmatrix} A_M + A_Z & A_V \\ 0 & A_D - A_V^T(A_M + A_Z)^\dagger A_V \end{bmatrix} \begin{bmatrix} U \\ V_L \end{bmatrix} = \begin{bmatrix} 0 \\ I^d \end{bmatrix} \tag{3.5.1}$$

Assuming $Y = (A_D - A_V^T(A_M + A_Z)^\dagger A_V)^\dagger$, then we have

$$YI^d = V_L \tag{3.5.2}$$

This is the matrix formulation of the discrete operator defined below. We define our discretized forward nonlinear mapping as

$$DF : \Delta\gamma|_\Omega \mapsto \Delta V|_{\partial\Omega} \tag{3.5.3}$$

or equivalently,

$$DF(\Delta\gamma) = \Delta V \tag{3.5.4}$$

where $\Delta\gamma$ and ΔV are discrete data.

Therefore, we could use (3.5.2) to calculate our voltage on the boundaries in simulations for

our forward problem. In this chapter, we firstly define the N-D, D-N mapping, the forward problem and corresponding inverse problem. Then, we discretize the forward problem by using FEM. Lastly we derive the matrix formulation of forward mapping in order to simulate the numerical experiments. For more details of discretization of EIT, see references [45, 46, 47, 48, 49, 50, 51, 52, 53]. In the next chapter, we will apply several iterative methods to solve our nonlinear inverse problem.

Chapter 4

Iterative methods

4.1 Basic principle of iterative methods

In this chapter, we note our EIT problem as nonlinear operator equations

$$F(x) = V \tag{4.1.1}$$

where $F : D(F) \subset X \to Y$ is a nonlinear operator between the spaces (i.e., Hilbert spaces) X and Y. x is the conductivity parameter. V is the calculated voltage on the boundary.

Similar to the discussion in last chapter, we would like to minimize our objective function as below,

$$f(x) = \frac{1}{2}(F(x) - V^{\delta}_{measure})^{*}(F(x) - V^{\delta}_{measure}) = \frac{1}{2}\left\|F(x) - V^{\delta}_{measure}\right\|_2^2 \tag{4.1.2}$$

where, we substitute the conductivity γ by x for clearer notation of discussing comparing with (3.3.1). To achieve our goal, we would like to apply very simple iterative idea by updating our x as the formula below,

$$x^{\delta}_{k+1} = x^{\delta}_{k} + \Delta x^{\delta}_{k}(x^{\delta}_{k}, V^{\delta}_{measure}),\ k \in N_0 \tag{4.1.3}$$

The different choice of Δx^{δ}_{k} that relates x^{δ}_{k} and $V^{\delta}_{measure}$ will be determined by various iterative methods.

In the linear case, we have a very simple iterative method, called Landweber iteration, to minimize the quadratic functional

$$\left\|Tx - y^{\delta}\right\|^2 \tag{4.1.4}$$

where T is a linear operator between spaces (i.e. Hilbert space) X and Y. Then we have Landweber iteration,

$$x^{\delta}_{k+1} = x^{\delta}_{k} + T^{*}(y^{\delta} - Tx^{\delta}_{k}) \tag{4.1.5}$$

In the nonlinear case, we replace Tx in functional (4.1.4) by $F(x)$ and assume our nonlinear forward mapping F has a continuous Fréchet-derivative $F'(\cdot)$, and replace y^{δ} by $V^{\delta}_{measure}$, we obtain

$$F'(x)^{*}(V^{\delta}_{measure} - F(x)) \tag{4.1.6}$$

as the negative gradient of the corresponding functional for nonlinear problems. Then, we get

the nonlinear Landweber iteration

$$x_{k+1}^{\delta} = x_k^{\delta} + F'(x_k)^*(V_{measure}^{\delta} - F(x_k^{\delta})) \tag{4.1.7}$$

The Landweber iteration above is easily realized numerically comparing with the following methods in the next sections. However, the number of iterations needed can be rather large. Therefore, one wants to find faster methods, and even the functional we need to minimize also should include the more prior information compared with (4.1.2). In a word, from this section, we know that the principle of iteration method is to find some ways to minimize our objective functional while updating unknown parameter x.

4.2 Newton type methods

4.2.1 Levenberg-Marquardt method

The method to solve the disadvantages of Landweber iteration is Levenberg-Marquardt method, which is very common.

Firstly, to find a x which minimizes $f(x)$ in (4.1.2), we set its derivative to zero, i.e.,

$$f'(x) = F'(x)^*(F(x) - V_{measure}^{\delta}) = 0 \tag{4.2.1}$$

where $[F'(x)]_{ij} = \partial F_i/\partial x_j$ and is called the Jacobian matrix.

We take the Taylor series expansion of $f'(x)$ at point x_k^{δ} and we have,

$$f'(x_{k+1}^{\delta}) = f'(x_k^{\delta}) + [f'(x_k^{\delta})]'\Delta x_k^{\delta} + \frac{1}{2}[f'(x_k^{\delta})]''(\Delta x_k^{\delta})^2 + O(\left\|(\Delta x_k^{\delta})^2\right\|) \tag{4.2.2}$$

where, $x_{k+1}^{\delta} = x_k^{\delta} + \Delta x_k^{\delta}$. Neglecting second order terms, yields

$$f'(x_{k+1}^{\delta}) \approx f'(x_k^{\delta}) + [f'(x_k^{\delta})]'\Delta x_k^{\delta} = 0 \tag{4.2.3}$$

The term f'' is called the Hessian matrix, expressed as

$$f'' = (F')^*F' + (F'')^*[I \otimes (F - V_{measure}^{\delta})] \tag{4.2.4}$$

where $\otimes$ is the Kronecker matrix product. When the desired minimum is approached, the second derivative term in (4.2.4) become negligible,

$$(F'')^*[I \otimes (F - V_{measure}^{\delta})] \simeq 0 \tag{4.2.5}$$

And, therefore,

$$f'' = (F')^*F' \tag{4.2.6}$$

Combing equation (4.2.1), (4.2.3) and (4.2.6), we finally have

$$\Delta x_k^{\delta} = [F'(x_k^{\delta})^*F'(x_k^{\delta})]^{-1}F'(x_k^{\delta})^*(V_{measure}^{\delta} - F(x_k^{\delta})) \tag{4.2.7}$$

Together with the basic iteration formula (4.1.3), we call this Newton-Raphson method.

However, it is worth noticing that $F'(x_k^\delta)^* F'(x_k^\delta)$ is ill-conditioned.

Alternatively, we can approximate the second term in (4.2.4) with λI rather than 0.

$$(F'')^*[I \otimes (F - V_{measure}^\delta)] \simeq \lambda I \tag{4.2.8}$$

Then, combining equation (4.2.1), (4.2.3), (4.2.4) and (4.2.8), we get

$$\Delta x_k^\delta = [F'(x_k^\delta)^* F'(x_k^\delta) + \lambda I]^{-1} F'(x_k^\delta)^* (F(x_k^\delta) - V_{measure}^\delta) \tag{4.2.9}$$

With iteration formula (4.1.3), this is Levenberg-Marquardt method.

4.2.2 Regularized Gauss-Newton method

In practice, the good way to maximize the convergence of the iteration process is to put maximal amount of prior knowledge into the process. At the start of the iteration process this prior knowledge is contained in the initial guess. But, the subsequent iterations should also be fed with prior knowledge. The idea is to put some constraint to the equation (4.1.2).

$$f(x) = \frac{1}{2} \left\| F(x) - V_{measure}^\delta \right\|_2^2 + \lambda^2 P(x) \tag{4.2.10}$$

where the second term, i.e., the penalty term, $P(x)$ takes the prior information into account. The smoothing parameter λ controls the relative weighting given to the prior information. If we assume our penalty term as the below, it is a well-known Tikhonov regularized functional.

$$f(x) = \frac{1}{2} \left\| F(x) - V_{measure}^\delta \right\|_2^2 + \frac{1}{2} \lambda^2 \left\| R(x^0 - x) \right\|_2^2 \tag{4.2.11}$$

where x^0 is the initial estimate of the solution. R is the regularization matrix which could have several structures. Therefore, our objective minimization functional is transformed from (4.1.2) into (4.2.11). Then, we can do the similar procedure as we did in the last section to get regularized Gauss-Newton formula.

Firstly, to find an x which minimizes $f(x)$ in (4.2.11), we set its derivative to zero, i.e.,

$$f'(x) = F'(x)^* (F(x) - V_{measure}^\delta) + \lambda^2 R^* R(x - x^0) = 0 \tag{4.2.12}$$

Then, considering the second derivative of equation (4.2.12), we yield

$$f'' = (F')^* F' + (F'')^* [I \otimes (F - V_{measure}^\delta)] + \lambda^2 R^* R \tag{4.2.13}$$

Here we approximate the second term of (4.2.13) to be zero like in equation (4.2.5), then we have the formulation of f''

$$f'' = (F')^* F' + \lambda^2 R^* R \tag{4.2.14}$$

Substituting (4.2.12) and (4.2.14) into (4.2.3), we yield

$$\Delta x_k^\delta = [F'(x_k^\delta)^* F'(x_k^\delta) + \lambda^2 R^* R]^{-1} [F'(x_k^\delta)^* (V_{measure}^\delta - F(x_k^\delta)) + \lambda^2 R^* R(x^0 - x)]$$

$$x_{k+1}^\delta = x_k^\delta + \Delta x_k^\delta \tag{4.2.15}$$

This formulation is regularized Gauss-Newton method which was introduced by Bakushinskii [54]. Further analysis in [54] shows that this has stabilizing properties on minimizing the functional. More details could also be found in [55].

4.3 Conjugate gradient type methods

4.3.1 CGNE method

As discussed in the last section, the steps of regularized Gauss-Newton method involve multiplying $(F')^*$ and F' times vectors, which needs very large storage in computing. And even computing the inverse of the large matrix in iterations would require more storage and be less efficient. One of the alternative methods for solving this problem is the conjugate gradient method, known as one of the most powerful algorithms for the solution of selfadjoint, positive (semi) definite well-posed linear equations. However, the less demand of storage and more efficient computation are advantages for us to consider this method in our problem.

For the description of the linear conjugate gradients on normal equations (CGNE) algorithm [21], the discrete linearized forward problem with noise contaminated measurements is considered

$$Jx^{\delta} = b \tag{4.3.1}$$

where J is the Jacobian of F and b the vector of differential boundary measurements. Unfortunately, when applied to the system (4.3.1), the implementation of the algorithm will have some problems, because the coefficients Jacobian matrix is neither symmetric nor positive definite. In order to apply CG method and get a reasonable rate of convergence, the transformation of the system (4.3.1) into a system of normal equations is important. Multiplying both sides of the equation with the transpose of J, the system of normal equation is formed as

$$J^*Jx^{\delta} = J^*b \tag{4.3.2}$$

However, this is not the end. It is important that the prior information about the solution and the measurements can still be imported into the inverse computations. A prior information matrix regarding the solution or image can be introduced as in the left side of the equation (4.3.2),

$$(J^*J + \lambda^2 R^*R)x^{\delta} = J^*b \tag{4.3.3}$$

where λ is the regularization parameter. R is the regularization matrix which could have several structures. For instances, R can be chosen as discrete Gaussian smoothing operator or discrete Laplace operator. The discrete Laplace operator is a 2nd order high pass filter that is a convolution with [58]

$$\begin{bmatrix} 1 & 1 & 1 \\ 1 & -8 & 1 \\ 1 & 1 & 1 \end{bmatrix} \text{ or } \begin{bmatrix} 0 & 1 & 0 \\ 1 & -4 & 1 \\ 0 & 1 & 0 \end{bmatrix}$$

on a rectangular mesh.

Then, if we define $A := \begin{bmatrix} J \\ \lambda R \end{bmatrix}$ and $y := \begin{bmatrix} b \\ 0 \end{bmatrix}$, we have the normal equation

$$A^* A x^\delta = A^* y \tag{4.3.4}$$

which can be applied to CG algorithm as the below,

Algorithm 4.3.1

- CG preparation:

x_0^δ= Some initial guess

$$r_0 = y - A x_0^\delta$$

$$p_1 = s_0 = A^* r_0$$

- CG iteration:

$$k = 1$$

While $\|r_i\|_2 > \varepsilon$ do

$$q_k = A p_k$$

$$\alpha_k = \|s_{k-1}\|^2 / \|q_k\|^2$$

$$x_k^\delta = x_{k-1}^\delta + \alpha_k p_k$$

$$r_k = r_{k-1} - \alpha_k p_k$$

$$s_k = A^* r_k$$

$$\beta_k = \|s_k\|^2 / \|s_{k-1}\|^2$$

$$p_{k+1} = s_k + \beta_k p_k$$

$$k = k + 1$$

End

4.3.2 NLCG method

The non-linear CG (NLCG) method [59] is considered to be one of the most efficient minimization algorithms used in both unconstrained and constrained optimization. In contrast to the Newton type methods which require first and second derivatives for the computation of the Newton direction, the computation of the direction in NLCG requires only that the function is smooth with continuous first derivatives.

- Basic principle

The basic idea of NLCG method is to minimize our functional $f(x)$ in (4.2.11) while updating our unknown conductivity parameter as the basic iteration formula below,

$$x_{k+1}^\delta = x_k^\delta + \alpha_k p_k \tag{4.3.5}$$

This is also a general form for the line search methods. Here x_k^δ is the kth iterate, p_k is the search direction, and α_k is (a scalar) step length parameter. An example of the line search methods is the steepest descent method

$$x_{k+1}^{\delta} = x_k^{\delta} - \alpha_k \nabla f(x_k^{\delta}) \tag{4.3.6}$$

where the search direction p_k is chosen to be the negative gradient $\nabla f(x_k^{\delta})$ which is known as the direction of the steepest descent. Usually, we need to compute the gradient $\nabla f(x_k^{\delta})$ in iterations. If the functional to be minimized is of the form (4.2.11), the gradient $\nabla f(x_k^{\delta})$ is

$$\nabla f(x_k^{\delta}) = J(x_k^{\delta})^*(F(x_k^{\delta}) - V_{measure}^{\delta}) + \lambda^2 R^* R(x - x^0) \tag{4.3.7}$$

However, in the simulation, the steepest descent method converges very slowly. So, updating step size and descent direction should be considered in iterations. In the next part, these two problems will be discussed.

- Search direction

In NLCG the steepest descent direction is chosen to be the first search direction and the next ones are linear combinations of the steepest descent direction $-\nabla f(x_k^{\delta})$ and the previous search direction p_{k-1}, that is,

$$p_k = -\nabla f(x_k^{\delta}) + \beta_k p_{k-1} \tag{4.3.8}$$

The choice of β_k could be as the following formulas,
*Fletcher-Reeves:

$$\beta_k^{FR} = \frac{\nabla f(x_k^{\delta})^* \nabla f(x_k^{\delta})}{\nabla f(x_{k-1}^{\delta})^* \nabla f(x_{k-1}^{\delta})} \tag{4.3.9}$$

*Polak-Ribière:

$$\beta_k^{PR} = \frac{\nabla f(x_k^{\delta})^* (\nabla f(x_k^{\delta}) - \nabla f(x_{k-1}^{\delta}))}{\nabla f(x_{k-1}^{\delta})^* \nabla f(x_{k-1}^{\delta})} \tag{4.3.10}$$

For more details about these two algorithms, see [60]. However, in the simulations of next chapter, we choose Fletcher-Reeves algorithm which has the better performance than Polak-Ribière in numerical experiments of our cases.

- Step size

When we have descended direction, the step size is chosen to minimize our objective functional $f(x_k^{\delta} + \alpha \nabla f(x_k^{\delta}))$ in (4.2.12). Thus we define,

$$\alpha_k := \arg\min_{\alpha} f(x_k^{\delta} + \alpha p_k) \tag{4.3.11}$$

In the algorithm, we perform the line search in this direction until it satisfies the Goldstein-conditions which is defined as below:
Choose α_k such that the actual decrease is of same magnitude as expected decrease,

$$f(x_{k+1}^{\delta}) - f(x_k^{\delta}) \leq \mu_1 \alpha_k \nabla f(x_k^{\delta})^* p_k \tag{4.3.12}$$

And additional condition is necessary to guarantee that α_k is not too small,

$$f(x_{k+1}^{\delta}) - f(x_k^{\delta}) \geq \mu_2 \alpha_k \nabla f(x_k^{\delta})^* p_k \tag{4.3.13}$$

The (4.3.12) and (4.3.13) are called Goldstein-conditions. And for more details of line search, see [61].

Finally, we summarize our NLCG algorithm,

- **Algorithm 4.3.2**

x_0^δ= Some initial guess

Evaluate $\nabla f(x_0^\delta)$

Set $p_0 = -\nabla f(x_k^\delta),\ k = 0$

While $\left\|F(x_k^\delta) - V_{measure}^\delta\right\|_2 > \epsilon$

Compute α_k by using line search according Goldstein-conditions

$x_{k+1}^\delta = x_k^\delta + \alpha_k p_k$

Evaluate $\nabla f(x_{k+1}^\delta)$

Compute β_{k+1} according (4.3.9) or (4.3.10)

$p_{k+1} = -\nabla f(x_{k+1}^\delta) + \beta_k p_k$

$k = k + 1$

End

Chapter 5

Simulations and discussions

In this chapter, in order to simulate the EIT problem by applying our reconstruction algorithms, we take several examples, such as 2D and 3D cases. The first section will discuss the 2D case and later section will study the 3D case. The software here we used is EIDORS toolkit for MATLAB [56]. All calculations were done on a laptop with an Intel Core i5-540M processor (2.53-Ghz, 3-MB smart cache, 2cores/4 threads) and 4GB (2*2GB) 1333 DDR3 ram.

5.1 Two dimensional numerical experiments

5.1.1 Model construction

In the 2D case, we take a 2D cylinder with 32 electrodes and inner two cylinders as the example.

At the beginning, we construct the model by using NETGEN software from Johannes Kepler University Linz as Figure 5.1.1.

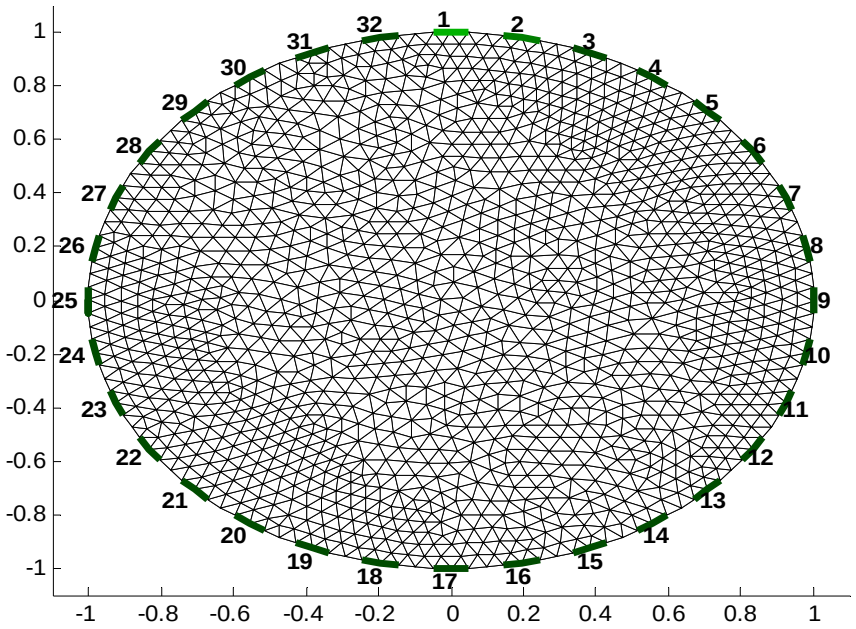

Figure 5.1.1 2D homogenous model with 32 electrodes

This is a model for solving our forward problem by using FEM. The total number of elements is 2676 with 1403 nodes. And we choose 32 electrodes on the boundary which are shown in green. Electrode#1 is light green. For conductivity distribution, we set the homogeneous conductivity for the whole model to be 1 for every element. And we add two cylinders into the model. The conductivity of these two objects is at 1.15 and 0.8 respectively for every element in the circles as in Figure 5.1.2.

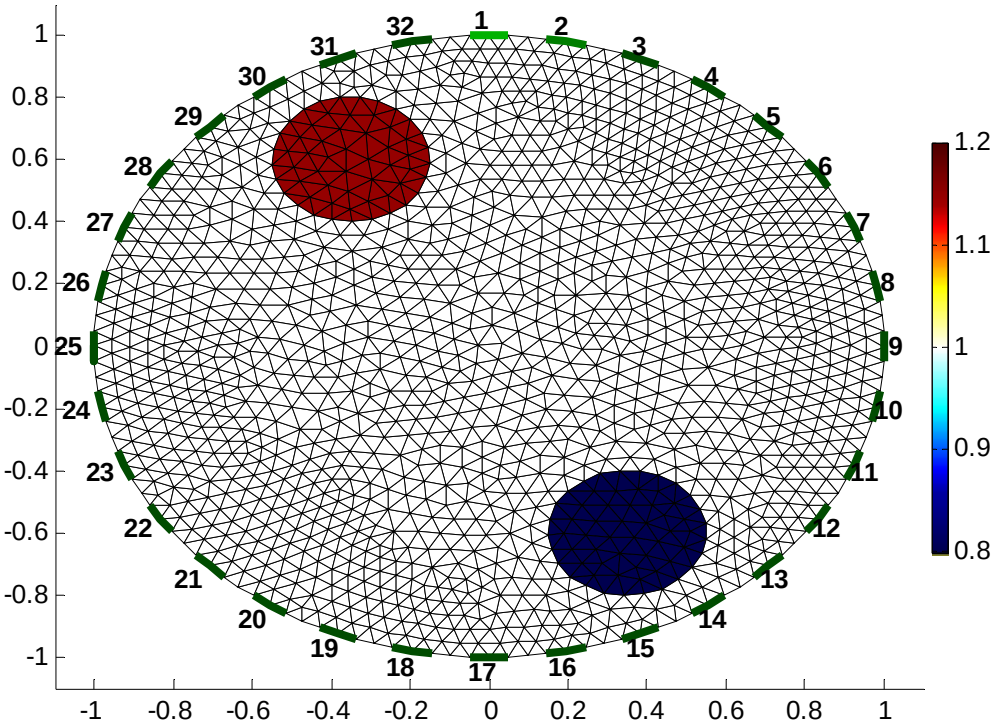

Figure 5.1.2 2D inhomogeneous model with 32 electrodes

Before simulating reconstruction, we need to choose the simulation pattern that is data collection method. Normally, there are two methods. One is the neighboring method and another is the opposite method that were roughly introduced in the chapter 2. Figure 5.1.3 illustrates the change of voltage pattern due to adding two objects by applying neighboring method. The first row shows the 1st stimulated voltage pattern. The left one is the voltage pattern without objects and the middle one is the voltage pattern with objects. The right is the difference in voltage pattern. The second row shows the 16th simulated voltage pattern. Figure 5.1.4 shows the voltage pattern by using the opposite method. The right column shows the voltage pattern in homogenous and the middle column is in inhomogeneous. The right column is the difference in voltage pattern. The top row is the 31st voltage pattern and the bottom row is the 15th voltage pattern. Because the opposite method has more uniform current density and hence good sensitivity, we choose this for our simulation pattern.

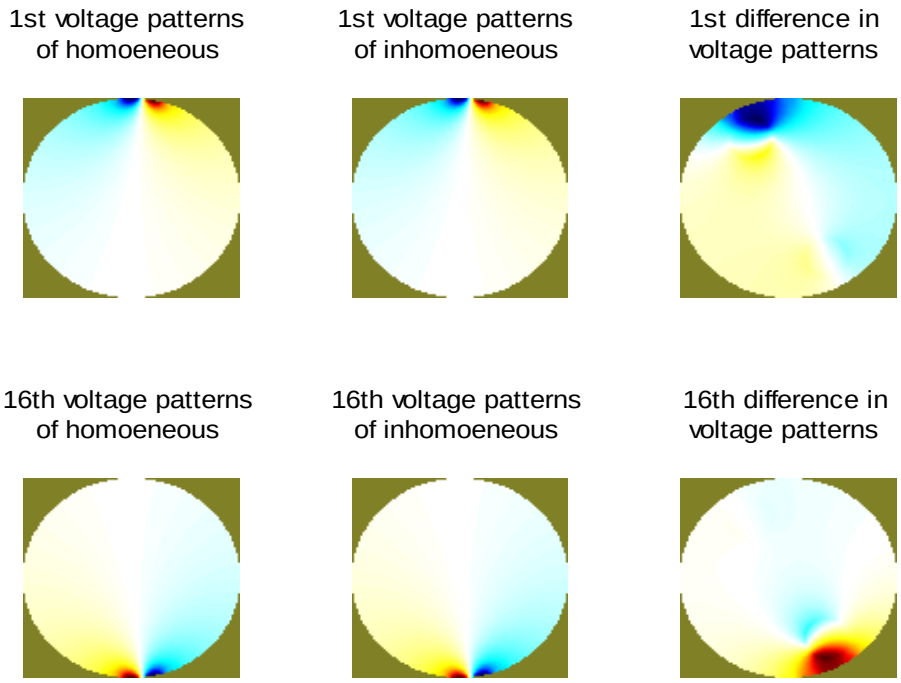

/

Figure 5.1.3 Voltage pattern in homogenous and inhomogeneous model (adjacent simulation)

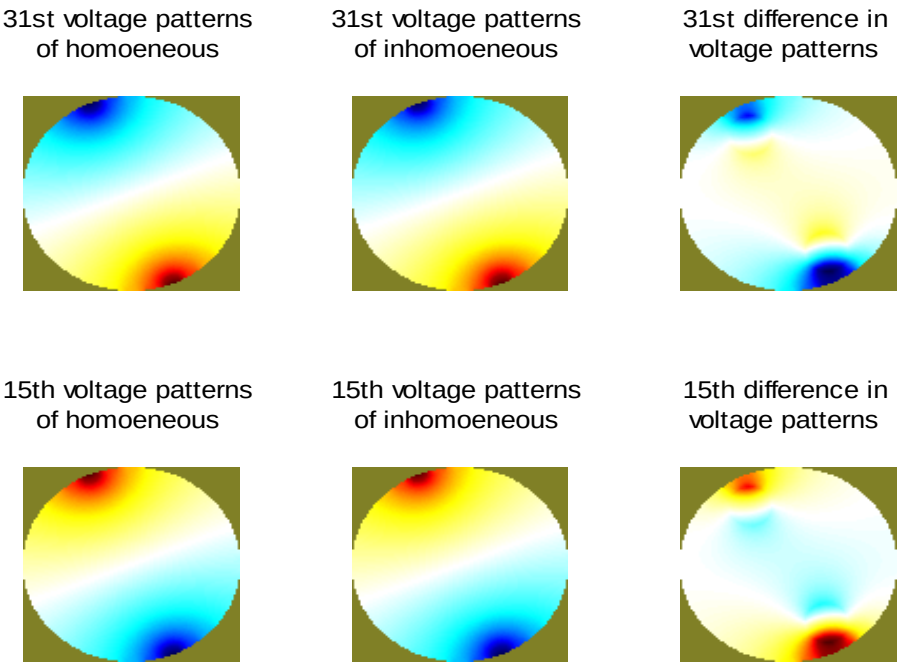

Figure 5.1.4 Voltage pattern in homogenous and inhomogeneous model (opposite simulation)

We could also observe the changes of simulated (measured) voltage on the boundary in Figure 5.1.5. The red axis (right) shows the range of the difference in voltage due to inhomogeneities. The red curve is the difference in voltage between the homogenous (green) and the inhomogeneous (blue) model.

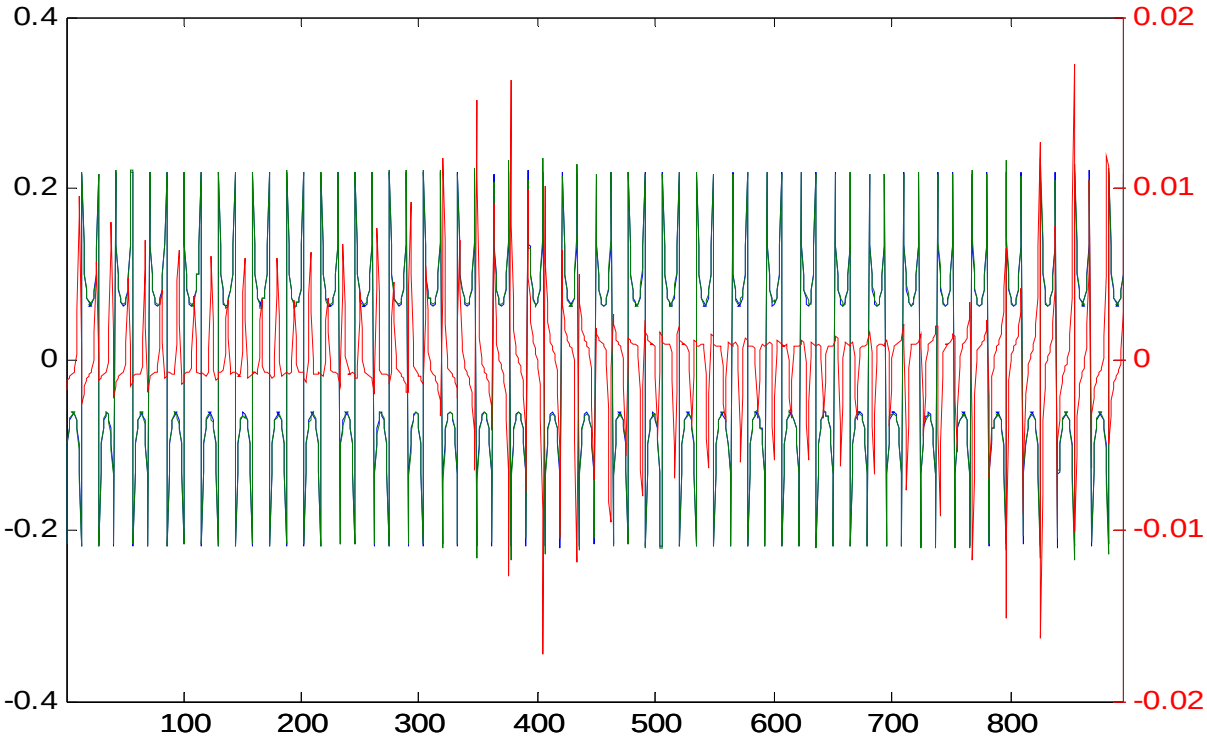

Figure 5.1.5 Simulated difference in voltage

5.1.2 Algorithm simulation

In this section we apply several algorithms which are introduced in the previous chapter for reconstructing the distribution of conductivity. In simulations, the regularization operator is chosen by Laplace operator which is a 2nd order high pass filter. The regularization parameter λ mentioned in the previous chapter is fixed by 0.01 and the initial guess is chosen to be zero. The stopping criterion is chosen as $\left\| F(x_k^\delta) - V_{measure}^\delta \right\|_2 < \varepsilon$.

- **Simulation without noise**

Firstly, we test our algorithms without noise. Figure 5.1.6 shows Landweber method (LW), regularized Gauss Newton method (RGN), conjugate gradient method for normal equation (CGNE) and nonlinear conjugate gradient method (NLCG) from left to right. At the top row, it shows the results of the algorithms which iterate two steps. In the case of LW, we could see the result is not good since the two reconstructed objects are near the boundary. RGN gives a very

good reconstruction compared with the real distribution of conductivity in Figure 5.1.2. CGNE is better than LW but even not as good as RGN. It seems that NLCG has the similar result of construction as CGNE. The bottom row illustrates that algorithms terminated at the tolerance ε=0.01 except LW which needs more steps and terminates at 200 iterations by setting manually. They stop at 200 (LW), 3 (RGN), 16 (CGNE) and 21 (NLCG) steps from left to right. LW does not change too much as well as RGN. However, CGNE and NLCG change a lot, although CGNE converges faster than NLCG.

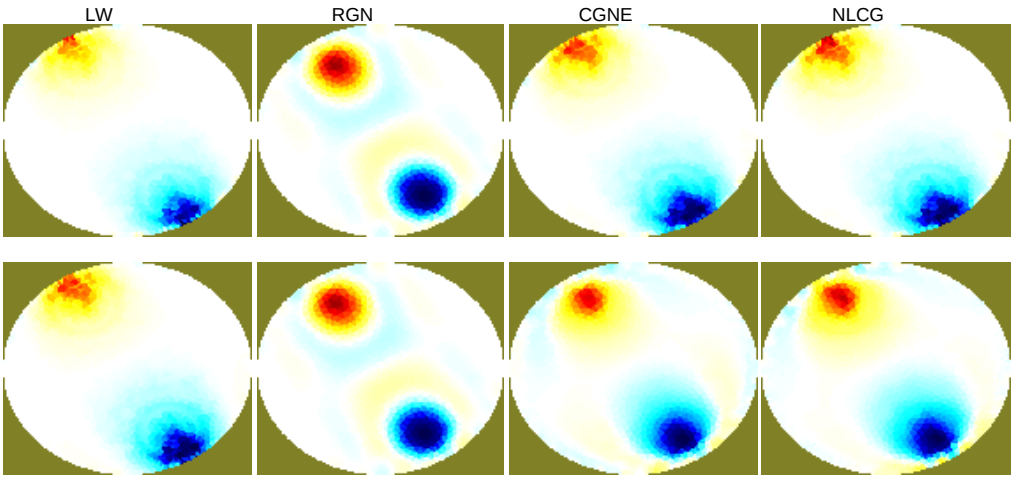

Figure 5.1.6 Comparison of different algorithms without noise

- **Simulation with noise**

In the real EIT test, the noise or measured errors is inevitable. To simulate the real case, we add 15dB noise into our simulated voltage of the inhomogeneous model. Figure 5.1.7 shows the changes of simulated (measured) voltage on the boundary with noise. Comparing with Figure 5.1.5, we could see there are more oscillations in the difference parts.

In Figure 5.1.8, the top row illustrates the algorithms with two steps. Comparing with the cases without noise in Figure 5.1.6 at the top row, LW has the similar result as it does without noise. However, the reconstructed distribution of conductivity by RGN is affected by noise much more than in Figure 5.1.6. There are not too many differences among cases of CGNE and NLCG for two steps iteration in Figure 5.1.6 and Figure 5.1.8. The bottom row shows the algorithms that iterates 50 steps. LW and RGN seem to have few changes. In contrast, the results of CGNE and NLCG are apparently changed after more iterations. The reconstructed two objects come closer into the center while the shapes of them become more rounded.

In Figure 5.1.9, we compared the speed of decrease in norm error of $\left\|F(x_k^\delta) - V_{measure}^\delta\right\|_2$ with different algorithms in the case with 15dB noise. It shows the fastest convergent rate is RGN, which is in blue dash dot line. The slowest convergent rate is LW which is in black plus line. For the other methods, CGNE in red dashed line is faster than NLCG in green dot line before

20th iteration. After that, NLCG become faster than CGNE, because we apply inexact line search to find the suitable step size for descent directions during the iteration and keep it decreasing as much as possible. However, NLCG and CGNE converge slower than RGN before 30th iteration, and then NLCG converges little faster than RGN.

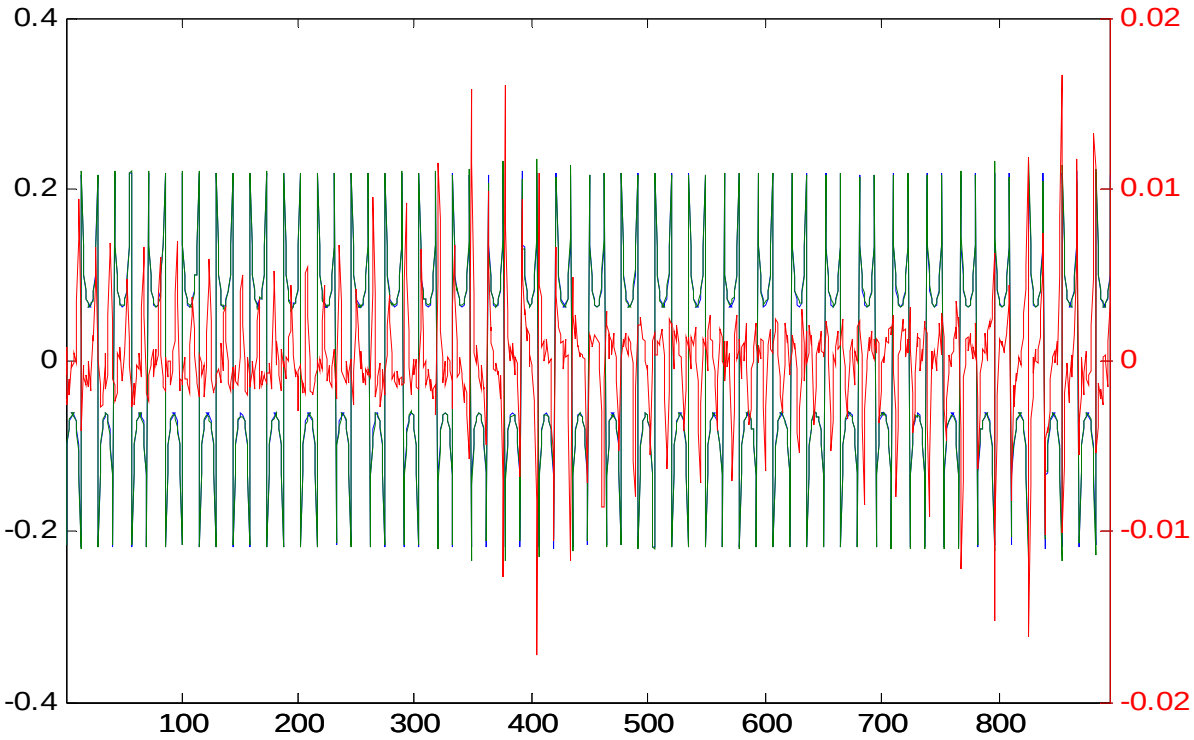

Figure 5.1.7 Simulated difference in voltage with 15dB noise

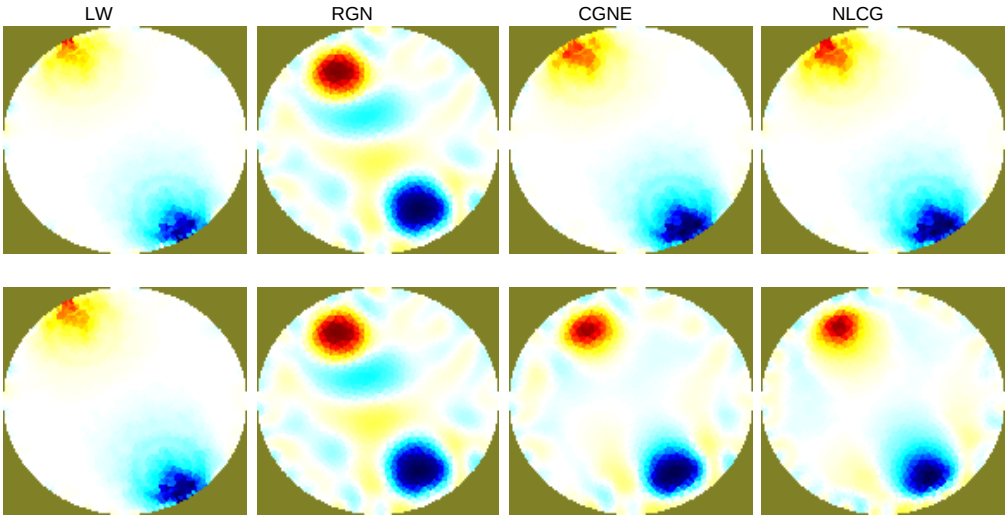

Figure 5.1.8 Comparison of different algorithms with noise

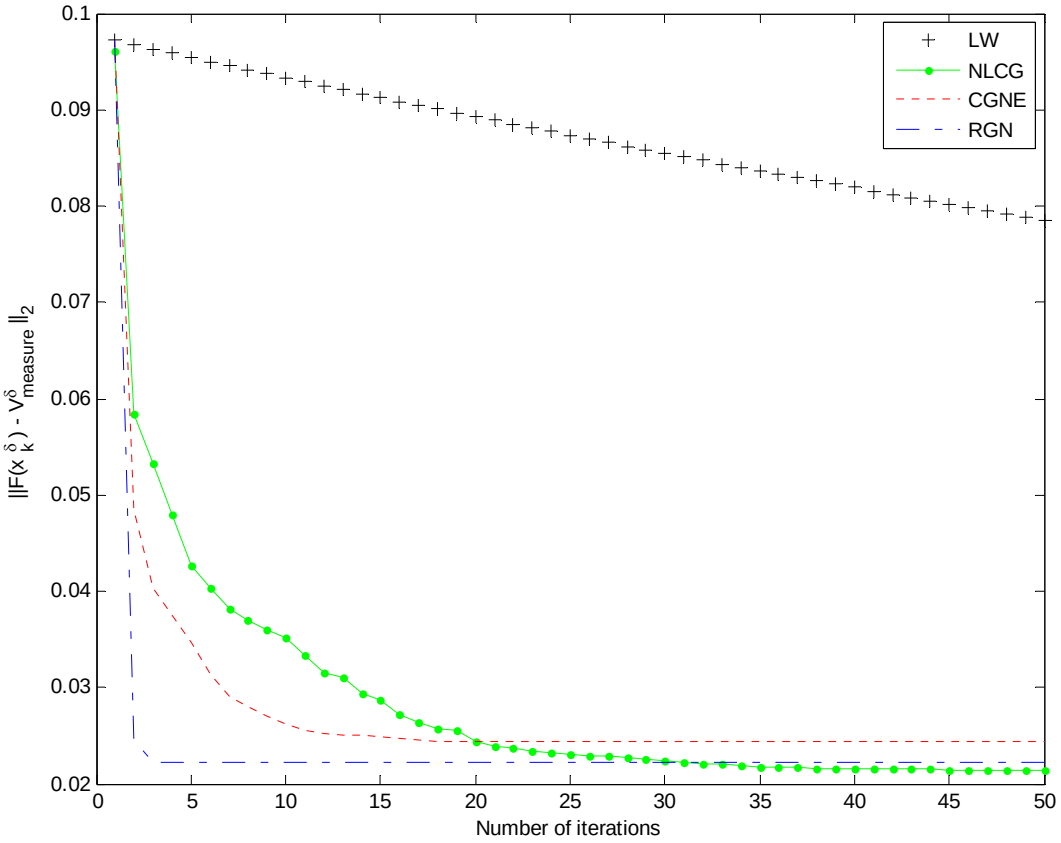

Figure 5.1.9 Decreasing rate of norm error in different algorithms with noise

- **Effects with different regularization parameter choice**

At the beginning of the experiments, we fixed our regularization parameter λ=0.01 by experiences. However, as we know, the value of the parameter will have some influences on our final reconstruction. Figure 5.1.10 illustrates the effects without noise for different values of λ^2 from the left to the right. At the top row, it shows the effects for one step RGN. When λ^2 equals 10^{-2}, it is not regularized very well since the distribution of conductivity of two objects are not very obvious compared with the cases in other parameter choices on the top. On the contrary, cases of one step NLCG at the bottom row seems not to be affected sensitively by the parameter choice in the range from 10^{-2} to 10^{-6}. In the middle row, it shows that the reconstruction of one step CGNE is not very well as λ^2 chosen by 10^{-2}, while this situation is changed by decreasing the value of parameter. In conclusion, the choice of 10^{-4} leads us to the expected results compared with our real distribution of conductivity. And 10^{-2} is worst choice among all.

In Figure 5.1.11, it shows changes of reconstruction by one step iteration, while the value of the parameter is decreasing from the left to the right base on adding the 15dB noise. At the top row, RGN's reconstruction of distribution of conductivity becomes more and more distinct until at 10^{-4} from the left to the right, and then the more inaccurate conductivity distribution

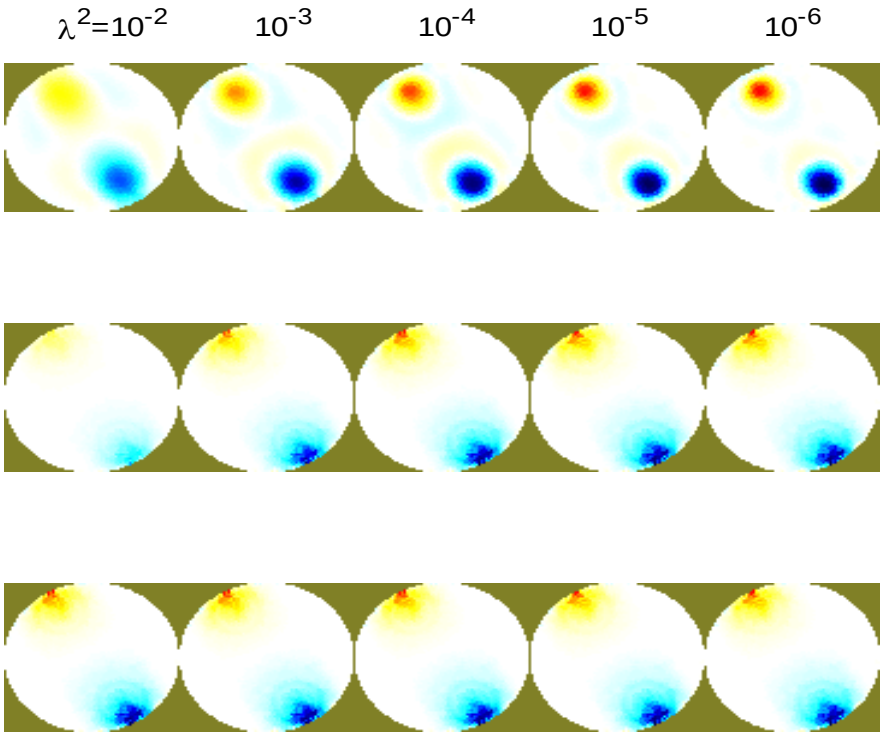

Figure 5.1.10 Effects on different parameters without noise

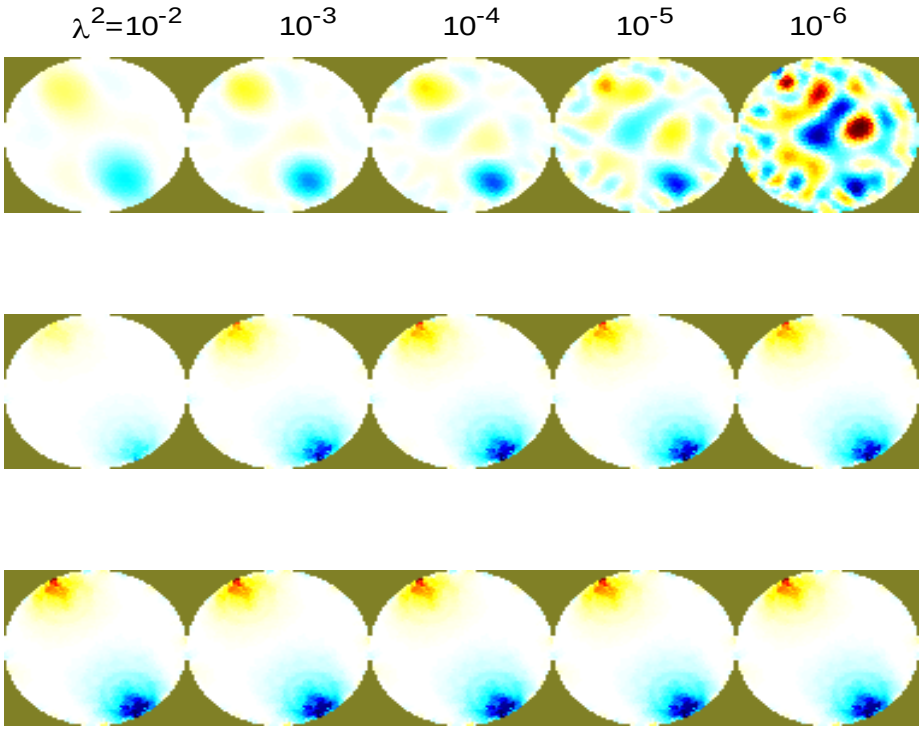

Figure 5.1.11 Effects on different parameters with noise

are added into the results of reconstruction. Especially at 10^{-6}, it achieves a totally wrong distribution which is affected much more other inaccurate distributions of conductivity. To the cases in the middle row for CGNE and at the bottom row for NLCG, the effects with different parameters with noise are not very different from the case without noise. In conclusion, the algorithm of RGN is more sensitivity than the other methods in the choice of parameter in cases with noise. Although, NLCG is not very sensitive, the parameter choice has effects on the step of line search during the iteration that may lead the line search to fail in further iterations. CGNE seems a compromise way with less sensitivity on parameter choice than RGN, while it has not disadvantage in failure of line search.

In a word, here, we choose the regularization parameter by visual inspection or experience, because the traditional methods for choosing the regularization parameter are not suitable in the case of EIT. It is worth to notice, however, that in the real case the use of visual examination is not possible, since the true conductivity distribution is unknown. The question of choosing the parameter in different cases is a topic of on-going research. But there are still some valuable heuristic methods for automatic parameter selection, see [57]. The aim of this thesis is not to consider this topic although we tentatively study the effects of election in regularization parameter for different algorithms in the previous parts. Therefore, it is the future work.

5.2 Three dimensional numerical experiments

5.2.1 Model construction

In this section, we only test CGNE and NLCG methods. Because large numbers of elements are needed in solving forward problem by FEM for 3D case, RGN is not very efficient computational method anymore. This is caused by the steps of iterations that RGN involves computing product of two large Jacobian matrix, while computing the inverse of the large matrix require large storage and would be less efficient computation. Actually, in the real experiments of EIT in 3D, the large matrix created by FEM has to be inevitable, since the accuracy of solution of forward problem is required. Therefore, CGNE and NLCG are alternative choices.

At the beginning, we construct the FEM model with Distmesh package as showing in Figure 5.2.1. The total number of elements is 7680 with 1595 nodes. And we choose 2 rings which has 16 green electrodes on the boundary of each one. Electrode#1 is light green. We set the homogeneous conductivity for the whole model as 1 for every element. And we add two objects into the model whose conductivity is at 1.15 and 0.8, respectively, for every element as in Figure 5.2.2.

Figure 5.2.3 shows three slices of cross-section for 3D inhomogeneous model at the levels of

z=0.3, z=0.1 and z=−0.2 from the left to the right, respectively.

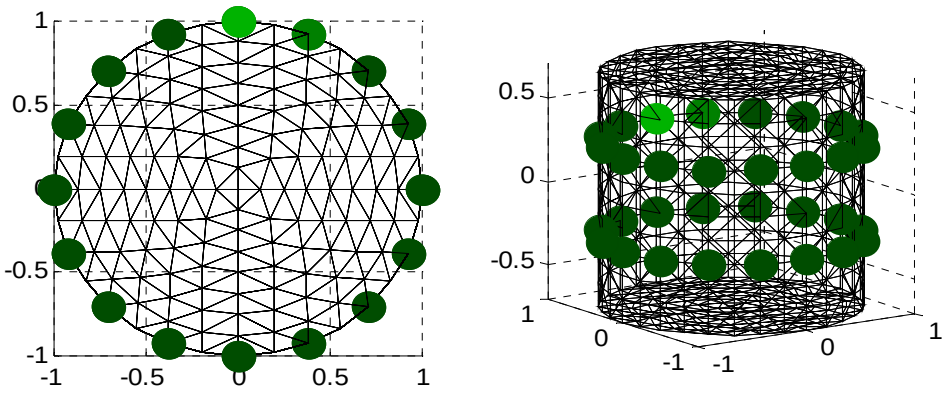

Figure 5.2.1 3D homogenous model with 2 rings and 32 electrodes

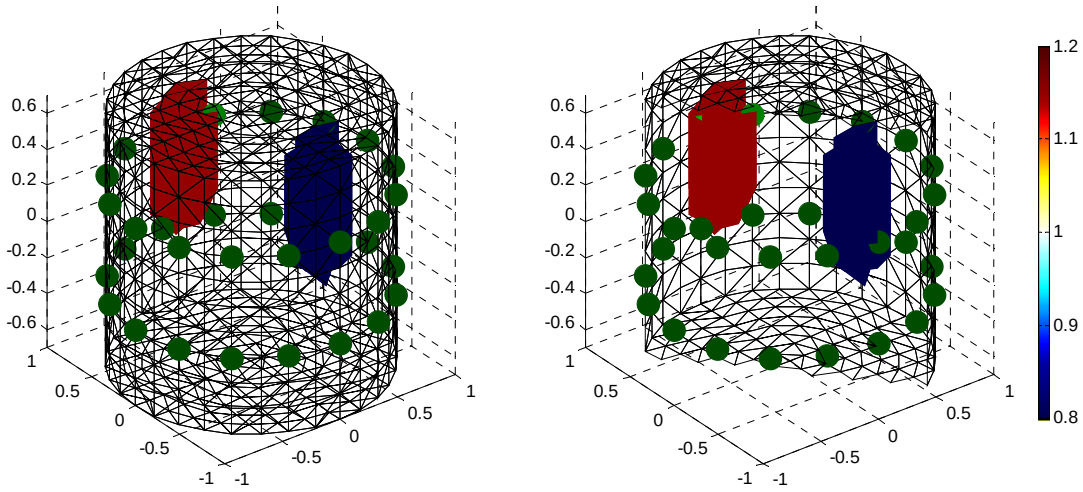

Figure 5.2.2 3D inhomogeneous model with 2 rings and 32 electrodes

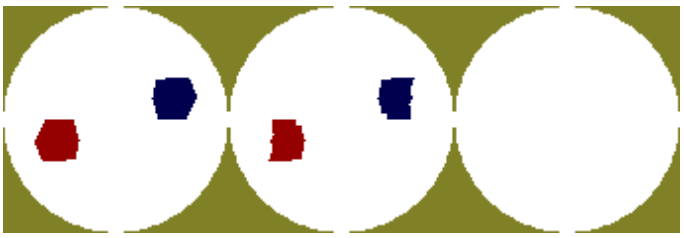

Figure 5.2.3 Three slices of inhomogeneous model

The same as in 2D case, simulation pattern will be determined before the algorithm simulation. Figure 5.2.4 to Figure 5.2.7 show changes of voltage due to adding two inhomogeneities. Figure 5.2.4 illustrates that 3 slices of the 1st voltage pattern of homogenous case (from top to bottom, z=0.3, z=0.1 and z=–0.2) is on the left and 3 slices of the 1st inhomogeneous is in the middle which are simulated by neighboring method. The right one is the difference between these two patterns. Figure 5.2.5 shows the 9th changes of voltage pattern. Figure 5.2.6 and Figure 5.2.7, show the 8th and 16th changes of voltage patterns, respectively, by applying opposite method. In these voltage pattern simulations, we observed that neighboring method is more suitable to our simulation pattern referring the true conductivity distribution in Figure 5.2.3

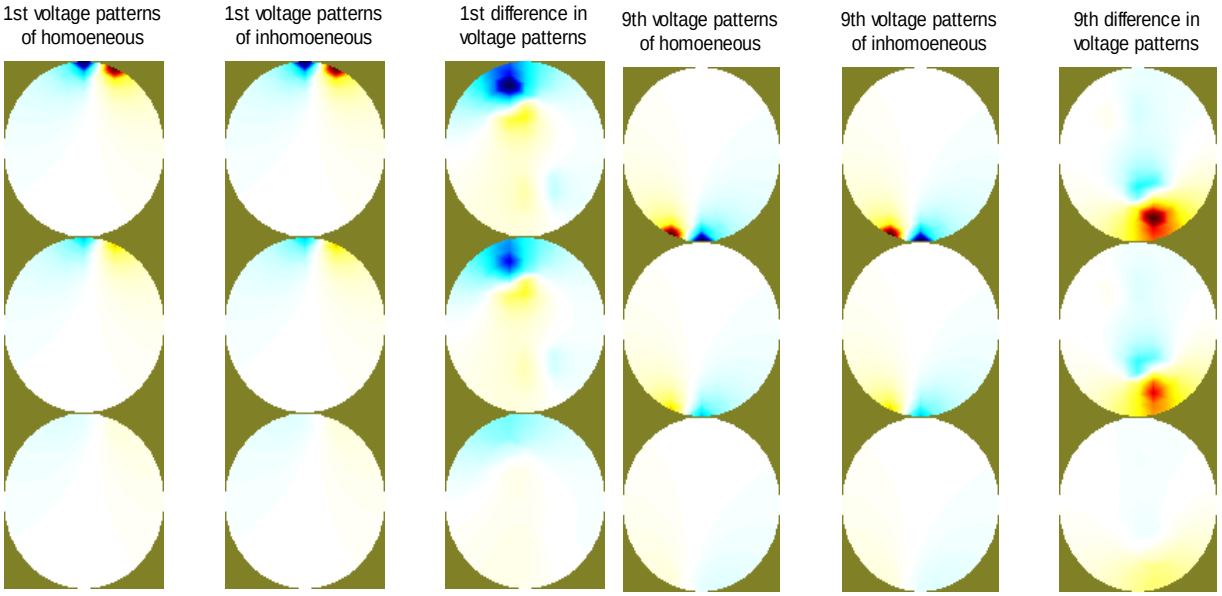

Figure 5.2.4

Figure 5.2.5

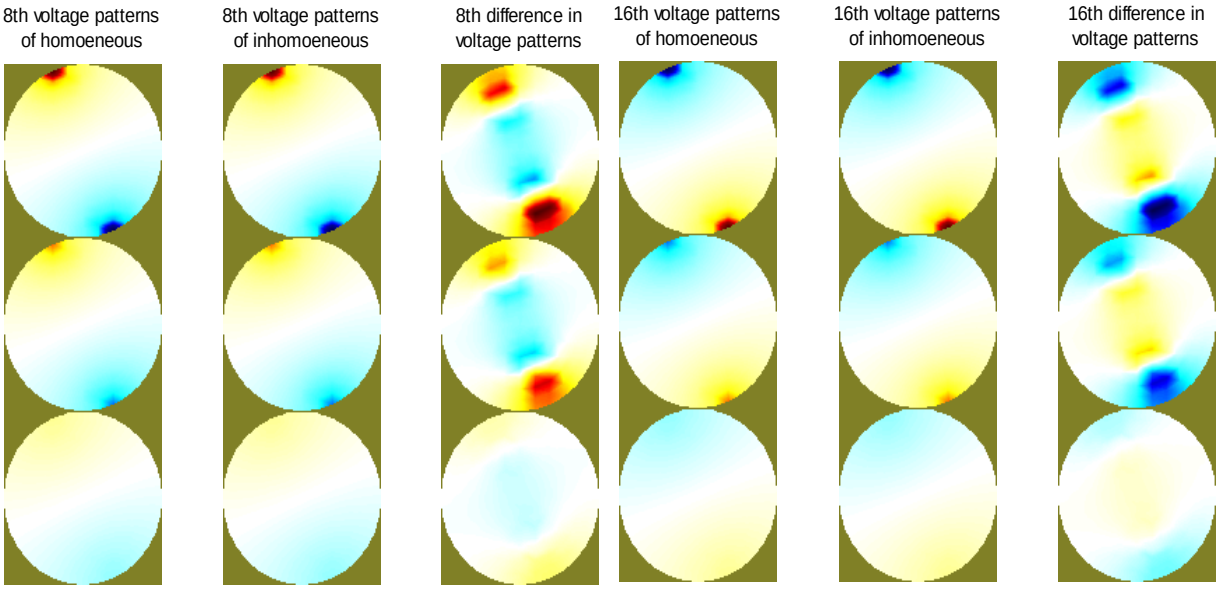

Figure 5.2.6

Figure 5.2.7

Therefore, the changes of simulated (measured) voltage on the boundary by applying neighboring method are shown in Figure 5.2.8.

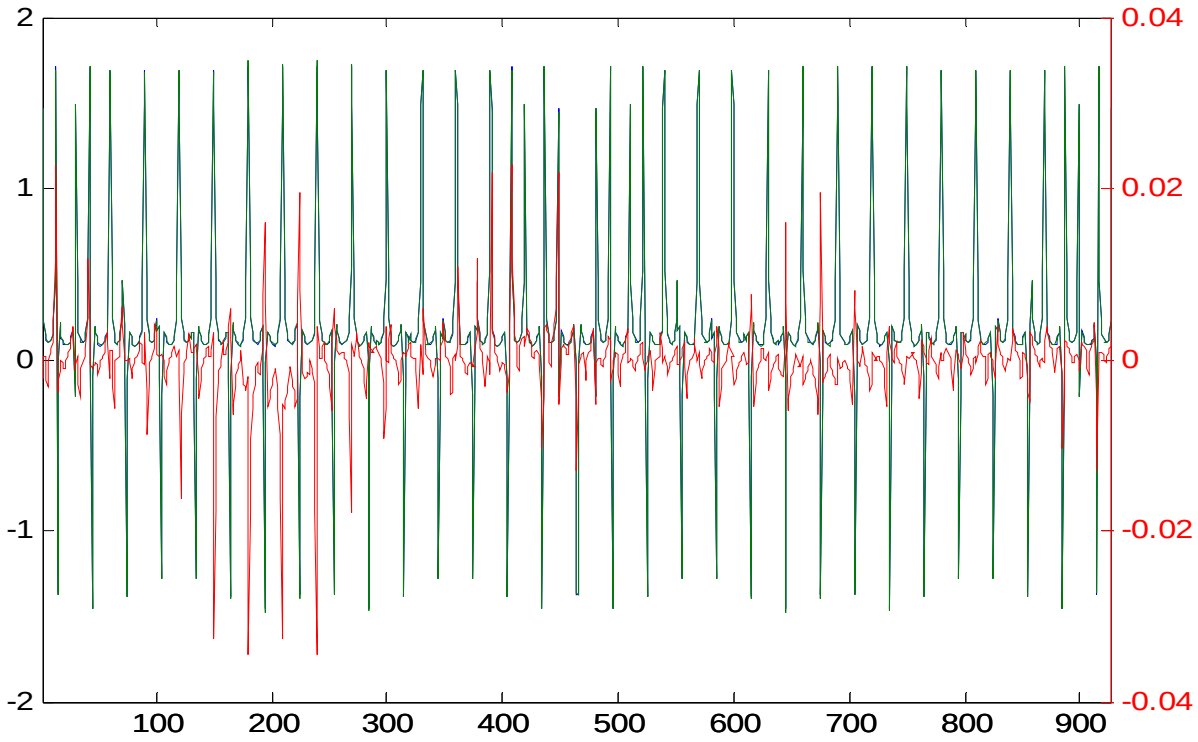

Figure 5.2.8 Simulated difference in voltage

We observe that the red axis (right) shows the range of the difference in voltage due to inhomogeneities. The red curve is the difference in voltage between homogenous (green) and inhomogeneous (blue) model.

5.2.2 Algorithm simulation

In this section we apply CGNE and NLCG for reconstructing the distribution of conductivity. In simulations, the regularization operator is chosen by Laplace operator which is a 2nd order high pass filter. The regularization parameter λ is fixed by 0.01 and the initial guess is chosen to be zero. The stopping criterion is chosen as norm error between the computed voltage and the simulated voltage (measured) which is smaller than the tolerance we set.

- **Simulation without noise**

Firstly, we test our algorithms without noise. Figure 5.2.9 shows 3 slices of reconstruction at z=0.3, z=0.1 and z=−0.2 from the top to bottom. CGNE and NLCG terminated at 38 iterates and 83 iterates respectively when setting ε=0.01. Compared with the true distribution of

conductivity, CGNE and NLCG seems to get good results but some wrong distribution appears on the boundary and on the slice at level of z=−0.2. Figure 5.2.10 illustrates 3D reconstruction by CGNE (in the middle) and NLCG (on the left). In conclusion, CGNE converges faster than NLCG.

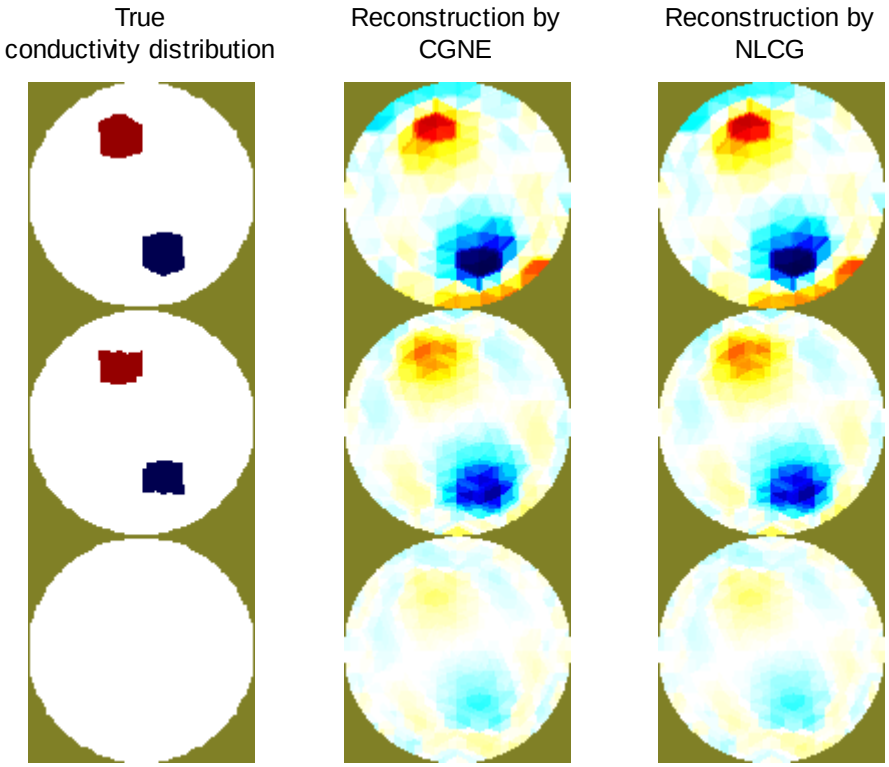

Figure 5.2.9 Reconstruction result of three slices in 3D case without noise

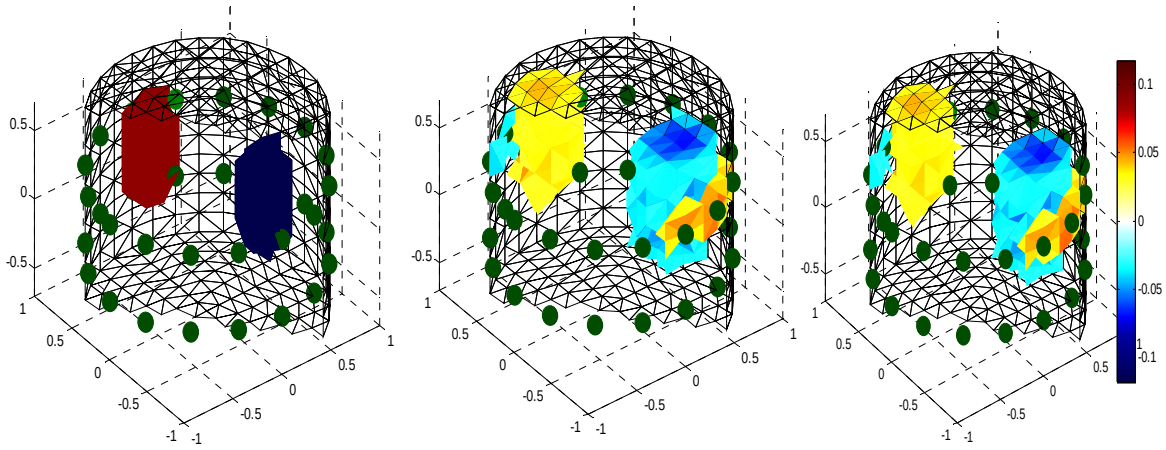

Figure 5.2.10 3D Reconstruction without noise

- **Simulation with noise**

In this case, we add 15dB noise into our simulated voltage of inhomogeneous model. Figure 5.2.11 shows the changes of simulated (measured) voltage on the boundary with noise. Comparing with Figure 5.2.8, we could see there are more oscillations in difference parts.

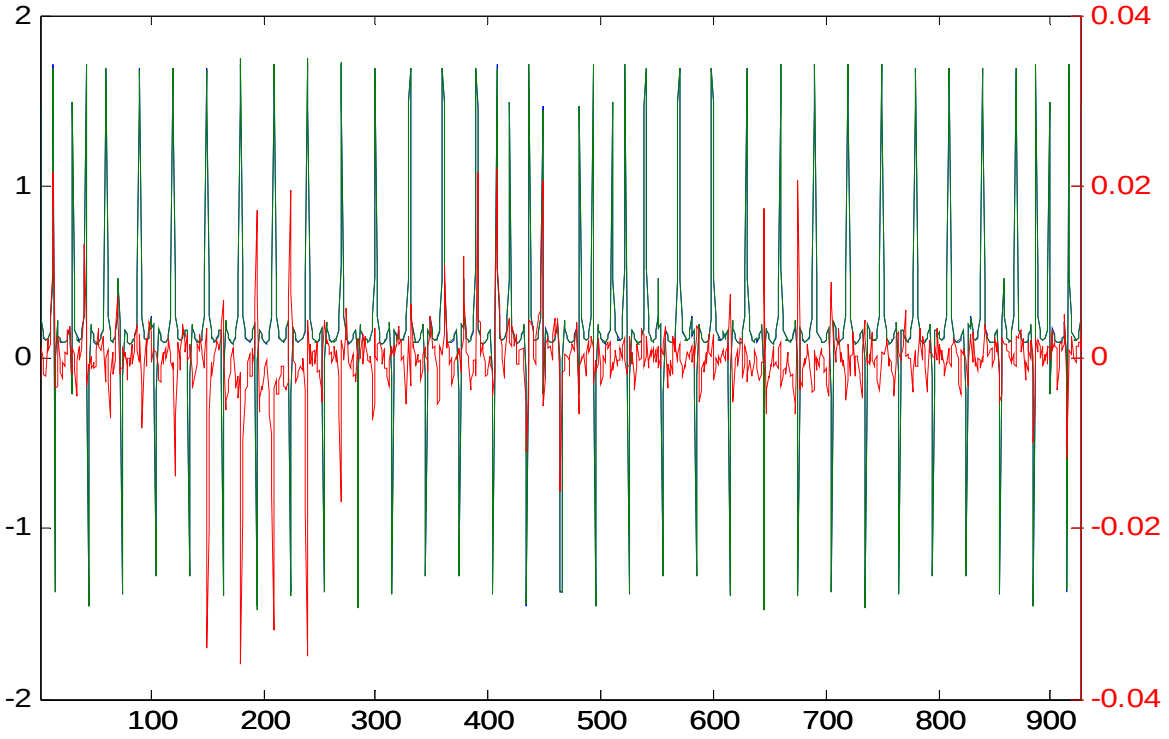

Figure 5.2.11 Simulated difference in voltage with 15dB noise

Figure 5.2.12 illustrates 3D reconstruction by CGNE (in the middle) and NLCG (on the left). In Figure 5.2.13, 3 slices of reconstruction at z=0.3, z=0.1 and z=−0.2 are shown from the top to bottom which are yielded by the true conductivity distribution, CGNE and NLCG from the left to the right, respectively. We terminated CGNE and NLCG at 100 iterations by setting the maximum iterations. However, compared with case without noise, the results of these two methods at 100 iterations are not very different. Only at z=−0.2, there are more wrong conductivity distributions.

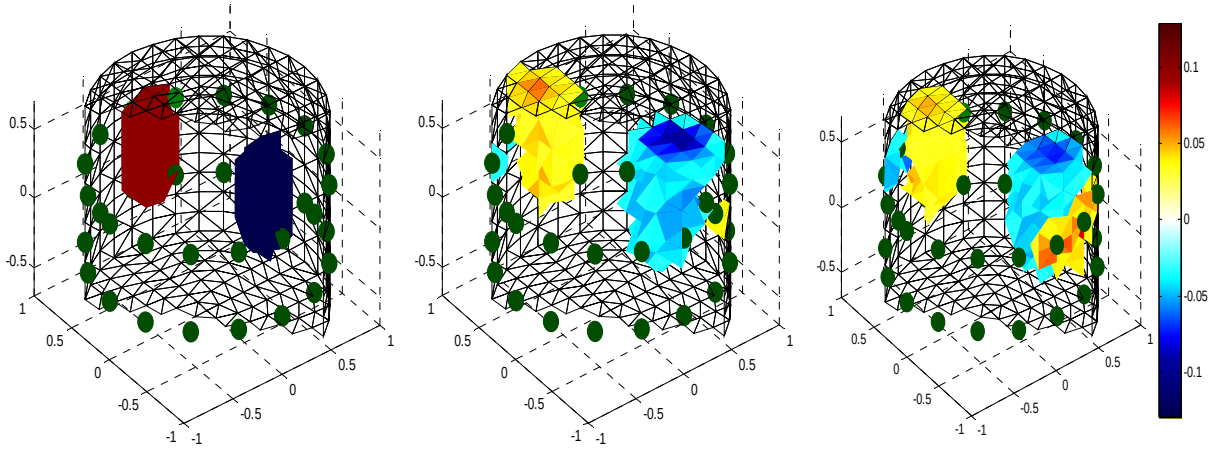

Figure 5.2.12 3D Reconstruction with noise

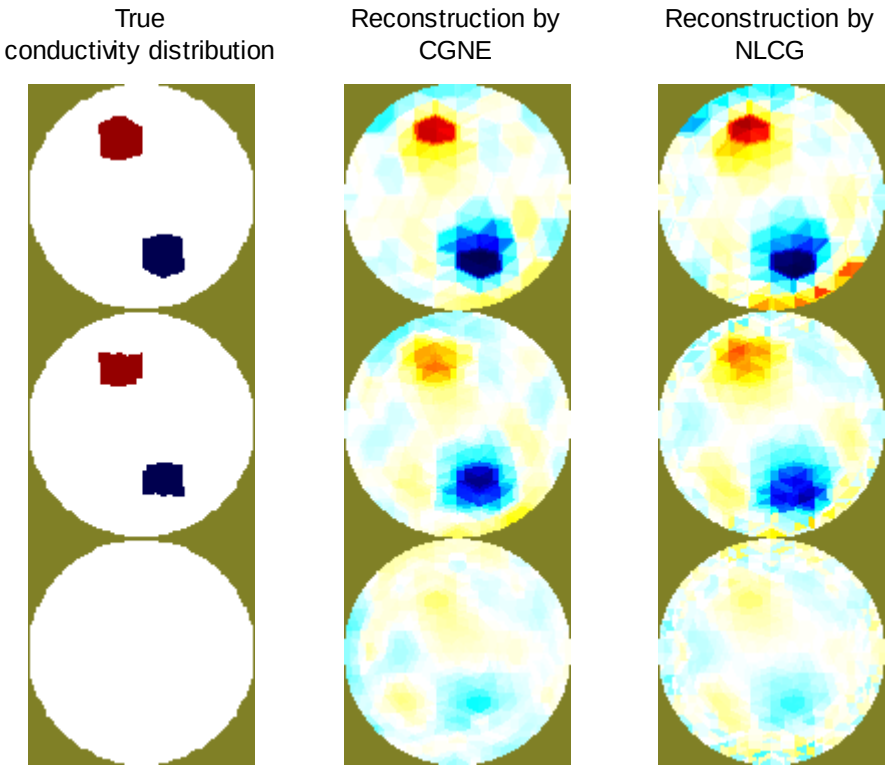

Figure 5.2.13 Reconstruction result of three slices in 3D case with noise

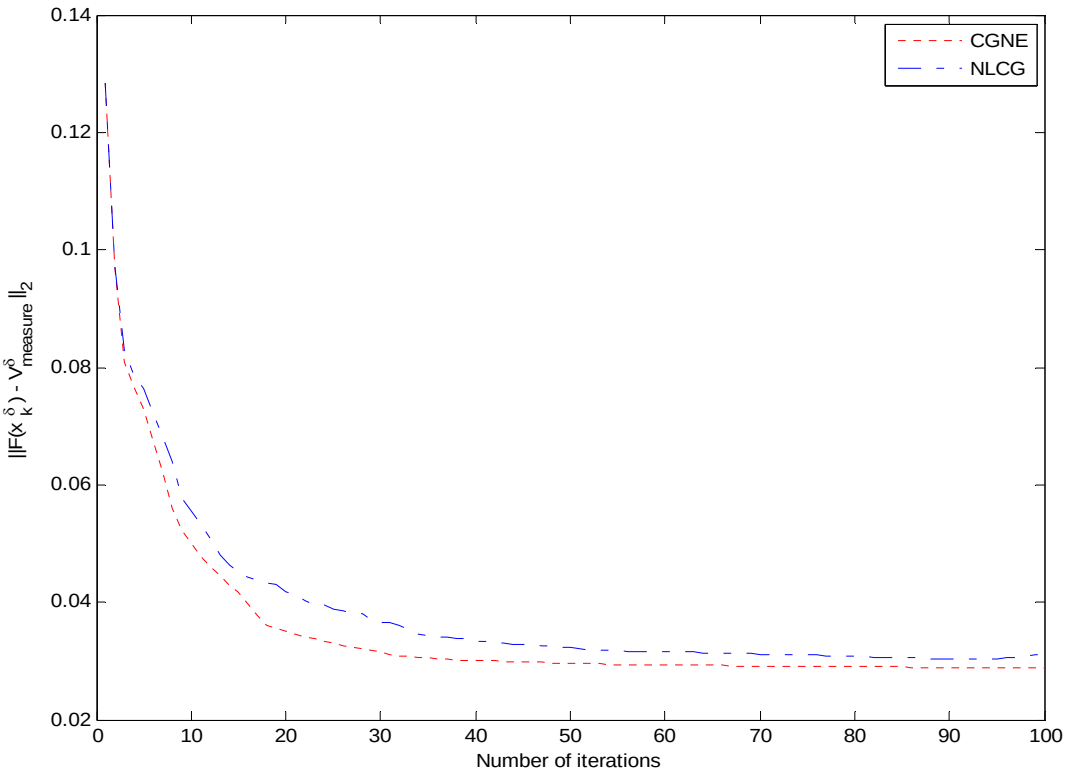

Figure 5.2.14 Decreasing rate of norm error in different algorithms with noise

In Figure 5.2.14, it compares the rate of decrease in norm error with CGNE and NLCG in the case with15dB noise. CGNE (in red dashed line) is faster than NLCG (in blue dash dot line). They decrease sharply before the 20th iterate, and then decline slowly.

In conlusion, CGNE is a more approiate choice for solving 3D case, because of the effiient computation in short time with less storage required. But NLCG needs more time in finding suitble step size in line search. In the last chapter, we make summaries with these algorithms and give some conclusions for this chapter.

Chapter 6

Conclusions and future work

6.1 Conclusions

In this study, we firstly studied the principle of EIT and derived the mathematical model for EIT reconstruction. We simply analyzed nonlinear ill-posedness of our inverse problem which means parameter estimation for partial differential equations. This made us clear that the method normally used in well-posed problem could not be suitable anymore and we decided regularized iterative methods for solving it. Then, we applied finite element method for solving the forward problem of EIT which is the significant part for the aim of reconstruction during applying iterative methods. After that, we studied several iterative methods which could be utilized in nonlinear ill-posed problem. In the part of simulation experiments, we applied some of these methods and discussed the results of them.

The object of this thesis is not only solving inverse problem of EIT by iterative methods but also studying which one is the better method in the specified case. In the 2D case, reconstructions with and without noise are studied. In Table 6.1.1, it shows efficiency of computation with different methods in the experiments of 2D reconstruction without noise, which was did in Chapter 5. In the situation with the same tolerance when $\varepsilon = 0.01$, the most efficiency method is RGN although CGNE computes faster. And the results of reconstruction shown in Figure 5.1.6 also illustrate RGN is the best one among these three methods. Table 6.1.2 shows different methods in computing time and iteration number with 2D noise case. It

2D reconstructions without noise	***CPU time(s)***	***Iteration number***	$\left\|F(x_k^\delta) - V_{measure}^\delta\right\|_2$
RGN	7.1	3	0.001223
CGNE	4.1	16	0.009837
NLCG	104.1	21	0.009544

Table 6.1.1

2D reconstructions with noise	***CPU time(s)***	***Iteration number***	$\left\|F(x_k^\delta) - V_{measure}^\delta\right\|_2$
RGN	222.6	50	0.021669
CGNE	26.5	100	0.023898
NLCG	612.3	100	0.022567

Table 6.1.2

seems NLCG is much less efficient than others. However, the noise effect on the final reconstruction of NLCG is the least shown in Figure 6.1.1. Therefore, NLCG is also a good alternative method for RGN and CGNE although it needs more CPU time.

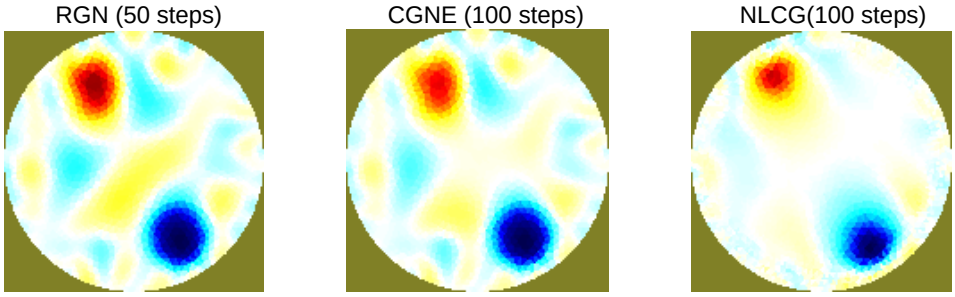

Figure 6.1.1

In the 3D experiments of Chapter 5, Table 6.1.3 and Table 6.1.4 show cases without and with noise respectively. Since RGN requires much more memory in 3D, it is not an efficient way anymore. Table 6.1.3 shows CGNE is much faster than NLCG and needs a small number of iteration when setting ε=0.01. In the case with noise, CGNE is also superior NLCG. Compared with reconstruction results without noise and with noise in Chapter 5, they have the similar good results. Therefore, CGNE is the suitable choice in the 3D reconstruction.

3D reconstructions without noise	***CPU time(s)***	***Iteration number***	$\left\|F(x_k^\delta) - V_{measure}^\delta\right\|_2$
CGNE	17.1	38	0.009896
NLCG	1703.9	83	0.009845

Table 6.1.3

3D reconstructions with noise	***CPU time(s)***	***Iteration number***	$\left\|F(x_k^\delta) - V_{measure}^\delta\right\|_2$
CGNE	36.7	100	0.028072
NLCG	1910.3	100	0.028906

Table 6.1.4

In conclusion, in the 2D EIT problem, if we know the exact relatively choice of the regularized parameter, RGN is a better option than others. If we could only know the range of the regularized parameter, NLCG could be a good choice. The reason of doing this is that RGN is more sensitive in regularized parameter than other two methods, which is discussed in Chapter 5. In the 3D EIT problem, CGNE is the best, but NLCG is also a good supplementary choice because of requiring less memory than RGN. It worth to notice, however, there are so many real applications that need us to choose the method depending on the model we construct.

6.2 Future works

In the last part, we summarize the work we need to do in the future. In this thesis, we studied several algorithms and simulated them. Finally, it gave some conclusions. However, because of having not enough time, there is still some space for improving and studying. So those ideas are suggested as the future works to do which have been listed below:

1) In the simulation, because traditional methods for choosing the regularization parameter are not suitable in the case of EIT, we fixed our regularization parameter value and selected it by experience and visual inspection. But this is not possible in the real EIT problem. So to find more suitable automatic selection method for regularization parameter is one of importance works to do.
2) In the simulation, we only applied the regularized operator by the Laplace operator. However, there are many cases need to apply other regularized operators to control prior information in reconstruction. So, studying more cases for different regularized operators is also important.
3) The model we simulated is not very complicated since it only has simple geometry shape. In the real EIT problem there are many cases that conductivity distributions are more complicated. So to study the efficiency of iterative methods in other complicated cases of EIT is very interested in the future work.
4) In the modeling part, we only restricted our model in direct current assumptions. However, some cases, i.e., geophysical problems need the model of alternating current which will be derived by the time dependent Maxwell equations. Studying the application in complex model is also challenging work.
5) In the simulation, we found the time consumed in the case of NLCG is much more. In fact, this because it takes too much time in line search for step size. To improve the efficiency of this step needs to be done.
6) The numbers of electrodes and their rings have some effects on reconstruction and iterative methods. To study these effects on EIT model mathematically is needed to be study as well.
7) There are also other iterative methods that provide possibilities to solve EIT reconstruction problem.

Generally speaking, I hope the work did in this thesis could be helpful for the later researchers in this field.

References

[1] H.W. Engl, A.K. Louis, and W. Rundell, *Inverse problems in geophysics*, SIAM, Philadelphia, 1996.

[2] M. Hanke, *A regularization Levenberg-Marquardt scheme, with application to inverse groundwater filtration problems*, Inverse Problems (1997), pp. 79-95.

[3] D. Zidarov, *Inverse gravimetric problem in geoprospecting and geodesy*, Elsevier, Amsterdam, 1980.

[4] J. Beck, B. Blackwell, and C.S. Clair, *Inverse heat conductions*, Wiley, Sussex, 1985.

[5] D.N. Hao and H.J. Reinhardt, *On a sideways parabolic equation*, Inverse problems (1997), pp. 297-309.

[6] D. Colton and R. Kress, *Inverse acoustic and electromagnetic scattering theory*, Springer, Berlin, 1992.

[7] J. Flusser, *On the inverse problem of rotation moment invariants*, Pattern Recognition (2002), pp. 35-86.

[8] M. Bertero and P. Boccacci, *Introduction to inverse problems in imaging*, Institute of Physics Publishing, London, 1998.

[9] G. Aubin and P. Kornprobst, *Mathematical problems in image processing*, Springer, Berlin, 2001.

[10] D. Isaacson and J.C. Newell, *Electrical impedance tomography*, SIAM Review (1999), pp. 85-101.

[11] H.W. Engl, A.K. Louis, and W. Rundell, *Inverse problems in medical imaging and nondestructive testing*, Springer, New York, Wien, 1996.

[12] F. Natterer, *The mathematics of computerized tomography*, Teubner, Stuttgart, 1986.

[13] B. Jacob, *Dynamics of fluids in porous media*, American Elsevier, New York (1972), pp. 214-215.

[14] J. A. Sethian and P. Smereka, *Level set methods for fluid interfaces*, Annual Review of Fluid Mechanics (2003), pp. 341-372.

[15] F. Black and M. Scholes, *The pricing of options and corporate liabilities*, Political Economy (1973), pp. 637-659.

[16] I. Bouchouev and V. Isakov, *Uniqueness, stability and numerical methods for the inverse problem that arises in financial markets*, Inverse Problems (1999), pp. 95-116.

[17] B. Dupire, *Pricing with a smile*, RISK (1994), pp. 18-20.

[18] H. Egger and H.W. Engl, *Tikhonov regularization applied to the inverse problem of option pricing: Convergence analysis and rates*, Inverse Problems (2005), pp. 1027-1045.

[19] J. Lishang and T. Youshan, *Identifying the volatility of underlying assets from option prices*, Inverse Problems (2001), pp. 137-155.

[20] J.Keller, *Inverse problems*, Amer. Math. Monthly 83 (1976), pp. 107-118.

[21] H.W. Engl, M. Hanke, and A. Neubauer, *Regularization of inverse problems*, Kluwer Academic, Dordrecht, 2000.

[22] J. Hadamard, *Lectures on the Cauchy problems in linear partial differential equations*, Yale University Press, New Haven, 1923.

[23] A.N. Tikhonov, A.S. Leonov, and A.G. Yagola, *Nonlinear ill-posed problems*, Chapman and Hall, 1995.

[24] A.M. Fedotov, *Linear ill-posed problems with random noise in the data*, Nauka, 1990.

[25] R.P. Feynman, R.B. Leighton, and M. Sands, *The Feynman lectures on physics*, 6th ed., vol. II, Addison-Wesley, Reading, 1977.

[26] M. Cheney, D.Isaacson, and J.C. Newell, *Electrical impedance tomography*, SIAM Review 41 (1999), no. 1, pp. 85-101.

[27] K. Paulson, W. Breckon, and M. Pidcock, *Electrode modeling in electrical impedance tomography*, SIAM Journal of Applied Mathematics 52 (1992), pp. 1012-1022.

[28] E. Somersalo, M. Cheney, and D. Isaacson, *Existence and uniqueness for electrode models for electric current computed tomography*, SIAM Journal of Applied Mathematics 52 (1992), pp. 1023-1040.

[29] R.W. Stacey, *Electrical impedance tomography*, Stanford Geothermal Program, Stanford University, 2006.

[30] J. Malmivuo and R. Plonsey, *Bioelectromagnetism*, Oxford University Press, 1995.

[31] I. Frerichs, T. Dudykevych, J. Hinz, M. Bodenstein, G. Hahn, and G. Hellige, *Gravity effects on regional lung ventilation determined by functional EIT during parabolic flights*, Journal of Applied Physiology 91 (2001), pp. 39-50.

[32] M. Vauhkonen, *Electrical impedance tomography and prior information*, Ph.D. thesis, University of Kuopio, Kuopio, 1997.

[33] V. Isakov, *Inverse problems for partial differential equations*, Springer, 1998.

[34] G. Alessandrini, *Stable determination of conductivity by boundary measurements*, Appl. Anal. 27 (1988), pp. 153-172.

[35] A. Allers and F. Santosa, *Stability and resolution analysis of a linearized problem in electrical impedance tomography*, Inverse Problems 7 (1991), pp. 515-533.

[36] A. Friedman and V. Isakov, *On the uniqueness in the inverse conductivity problem with one measurement*, Indiana University, Math. J. 38 (1989), pp.563-579.

[37] V. Isakov, *On uniqueness of recovery of discontinuous conductivity coefficients*, Comm. Pure Appl. Math. 47 (1988), pp. 864-876.

[38] V. Isakov and J. Powell, *On the inverse conductivity problem with one measurement*, Inverse Problems 6 (1990), pp.311-318.

[39] A. Nachman, *Global uniqueness for the two-dimensional inverse boundary value problem*, Ann. of Math. 142 (1995), pp. 71-96.

[40] O. Scherzer, *The use of Tikhonov regularization in the identification of electrical conductivities from overdetermined boundary data*, Results Math. 22 (1992), pp. 598-618.

[41] E. Somersalo, D. Isaacson, and M. Cheney, *Existence and uniqueness for electrode models for electric current computed tomography*, SIAM J. Appl. Math. 52 (1992), pp. 1023-1040.

[42] J. Sylvester and G. Uhlmann, *Inverse boundary value problems at the boundary - Continuous dependence*, Comm. Pure Appl. Math. 41 (1988), pp. 197-219.

[43] A. Trächtler, *A fast non-linear reconstruction technique for electrical impedance tomography*, Proceedings of the Frontiers in Industrial Process Tomography Ⅱ, 1997.

[44] P.P. Sylvester and R.L. Ferrari, *Finite elements for electrical engineers*, Cambridge University Press, Cambridge, 2001.

[45] O. Dorn, H. Bertete-Aguirre, J.C. Berryman, and G.C. Papanicolaou, *A non-linear inversion method for 3D electromagnetic imaging using adjoint fields*, Inverse Problems 15, 1999.

[46] R. Gadd, F. Vinther, P.M. Record, and P. Rolfe, *Reconstruction of three-dimensional data for electrical impedance tomography*, Electronic Letters 28, 1992.

[47] J.C. Goble, D.G. Gisser, D. Isaacson, and J.C. Newell, *Electrical impedance tomography in three*

dimensions, Proceedings of the Biomedical Engineering Society conference, 1990.

[48] J.C. Goble, *The three-dimensional inverse problem in electric current computed tomography*, Ph.D. thesis, Rensselaer Polytechnic Institute, New York, 1990.

[49] J.C. Goble, M. Cheney and D. Isaacson, *Electrical impedance tomography in three dimensions*, Applied Computational Electromagnetics 7 (1992), pp. 128-147.

[50] A. Le Hyaric and M.K. Pidcock, *A single step image reconstruction algorithm for electrical impedance tomography in three dimensions*, Physiological Measurement 21, 2000.

[51] P.A.T. Pinheiro, W.W. Loh and F. Dickin, *Three-dimensional reconstruction algorithm for electrical resistance tomography*, Proceedings of IEE Science of Measurement and Technology 145, 1998.

[52] N. Polydorides, *Image reconstruction algorithms for soft-field tomography*, Ph.D. thesis, University of Manchester Institute of Science and Technology, Manchester, 2002.

[53] A. Wexler, *Electrical impedance imaging in two and three dimensions*, Clinical Physics and Physiological Measurement 9, 1988.

[54] A. B. Bakushinskii, *The problem of the convergence of the iteratively regularized Gauss-Newton method*, Computational Mathematics and Physics 32 (1992), pp.1353-1359.

[55] B. Kaltenbacher, A. Neubauer, and O. Scherzer, *Iterative regularization methods for nonlinear ill-posed problems*, Radon Series on Computational and Applied Mathematics, de Gruyter, Berilin, 2008

[56] A. Adler and W. R B Lionheart, *Uses and abuses of EIDORS: An extensible software base for EIT*, Physiol. Meas. 27:S25-S42, 2006.

[57] B. M. Graham and A. Adler, *Objective selection of hyperparameter for EIT*, Physiol. Meas. 27:S65-S79, 2006.

[58] Wikipedia, http://en.wikipedia.org/wiki/Discrete_Laplace_operator, 19-06-2011.

[59] Wikipedia, http://en.wikipedia.org/wiki/Nonlinear_conjugate_gradient, 19-06-2011.

[60] J. Nocedal and S.J. Wright. *Numerical Optimization*, Springer series in operations reseach. Springer-Verlag, New York, 1999.

[61] H. Gfrerer, *Lecture notes on optimization*, Johannes Kepler University, Linz, Austria, 2009.